The oxysterol–CXCR2 axis plays a key role in the recruitment of tumor-promoting neutrophils

Laura Raccosta,[1] Raffaella Fontana,[1] Daniela Maggioni,[1] Claudia Lanterna,[1] Eduardo J. Villablanca,[2] Aida Paniccia,[1] Andrea Musumeci,[1] Elena Chiricozzi,[3] Maria Letizia Trincavelli,[4] Simona Daniele,[4] Claudia Martini,[4] Jan-Ake Gustafsson,[5,6] Claudio Doglioni,[7,8] Safiyè Gonzalvo Feo,[9] Andrea Leiva,[1] Maria Grazia Ciampa,[3] Laura Mauri,[3] Cristina Sensi,[10] Alessandro Prinetti,[3] Ivano Eberini,[10] J. Rodrigo Mora,[2] Claudio Bordignon,[8,11] Knut R. Steffensen,[5] Sandro Sonnino,[3] Silvano Sozzani,[9,12] Catia Traversari,[11] and Vincenzo Russo[1]

[1]Cancer Gene Therapy Unit, Program of Immunology and Bio Immuno Gene Therapy of Cancer, Division of Molecular Oncology, and [7]Department of Pathology, Scientific Institute San Raffaele, 20132 Milan, Italy
[2]Gastrointestinal Unit, Massachusetts General Hospital, Boston, MA 02114
[3]Department of Medical Chemistry, Biochemistry and Biotechnology, Center of Excellence on Neurodegenerative Diseases, University of Milan, 20090 Segrate, Italy
[4]Department of Pharmacy, University of Pisa, 56126 Pisa, Italy
[5]Department of Biosciences and Nutrition, Karolinska Institute, S-14183 Huddinge, Sweden
[6]Center for Nuclear Receptors and Cell Signaling, University of Houston, Houston, TX 77204
[8]Università Vita-Salute San Raffaele, 20132 Milan, Italy
[9]Humanitas Clinical and Research Center, 20089 Rozzano, Italy
[10]Proteomics and Protein Structure Study Group, Department of Pharmacological Sciences, University of Milan, 20133 Milan, Italy
[11]MolMed S.p.A., 20132 Milan, Italy
[12]Department of Molecular and Translational Medicine, University of Brescia, 25123 Brescia, Italy

Tumor-infiltrating immune cells can be conditioned by molecules released within the microenvironment to thwart antitumor immune responses, thereby facilitating tumor growth. Among immune cells, neutrophils play an important protumorigenic role by favoring neoangiogenesis and/or by suppressing antitumor immune responses. Tumor-derived oxysterols have recently been shown to favor tumor growth by inhibiting dendritic cell migration toward lymphoid organs. We report that tumor-derived oxysterols recruit protumor neutrophils in a liver X receptor (LXR)–independent, CXCR2-dependent manner, thus favoring tumor growth by promoting neoangiogenesis and immunosuppression. We demonstrate that interfering with the oxysterol–CXCR2 axis delays tumor growth and prolongs the overall survival of tumor-bearing mice. These results identify an unanticipated protumor function of the oxysterol–CXCR2 axis and a possible target for cancer therapy.

CORRESPONDENCE
Vincenzo Russo:
v.russo@hsr.it

Abbreviations used: CM, conditioned medium; GPCR, G protein–coupled receptor; LLC, Lewis lung carcinoma; LXR, liver X receptor; MS, mass spectrometry; PTX, pertussis toxin; SULT2B1b, sulfotransferase 2B1b.

Tumor formation is the result of molecular alterations involving cellular regulators (Hanahan and Weinberg, 2011) as well as the ability of tumor cells to affect the tumor microenvironment by smoldering inflammation (de Visser et al., 2006; Mantovani et al., 2008) or even taking advantage of inflammation to grow and metastasize (Zitvogel et al., 2006; Grivennikov et al., 2010). Indeed, targeted therapies aimed to inhibit molecular alterations in tumor cells even though inducing antitumor responses have improved overall survival only slightly, indicating that antitumor strategies comprehensive of drugs targeting molecular as well as microenvironment alterations might be more effective

R. Fontana and D. Maggioni contributed equally to this paper.
C. Traversari and V. Russo contributed equally to this paper.

The Rockefeller University Press $30.00
J. Exp. Med. 2013 Vol. 210 No. 9 1711-1728
www.jem.org/cgi/doi/10.1084/jem.20130440

The Journal of Experimental Medicine

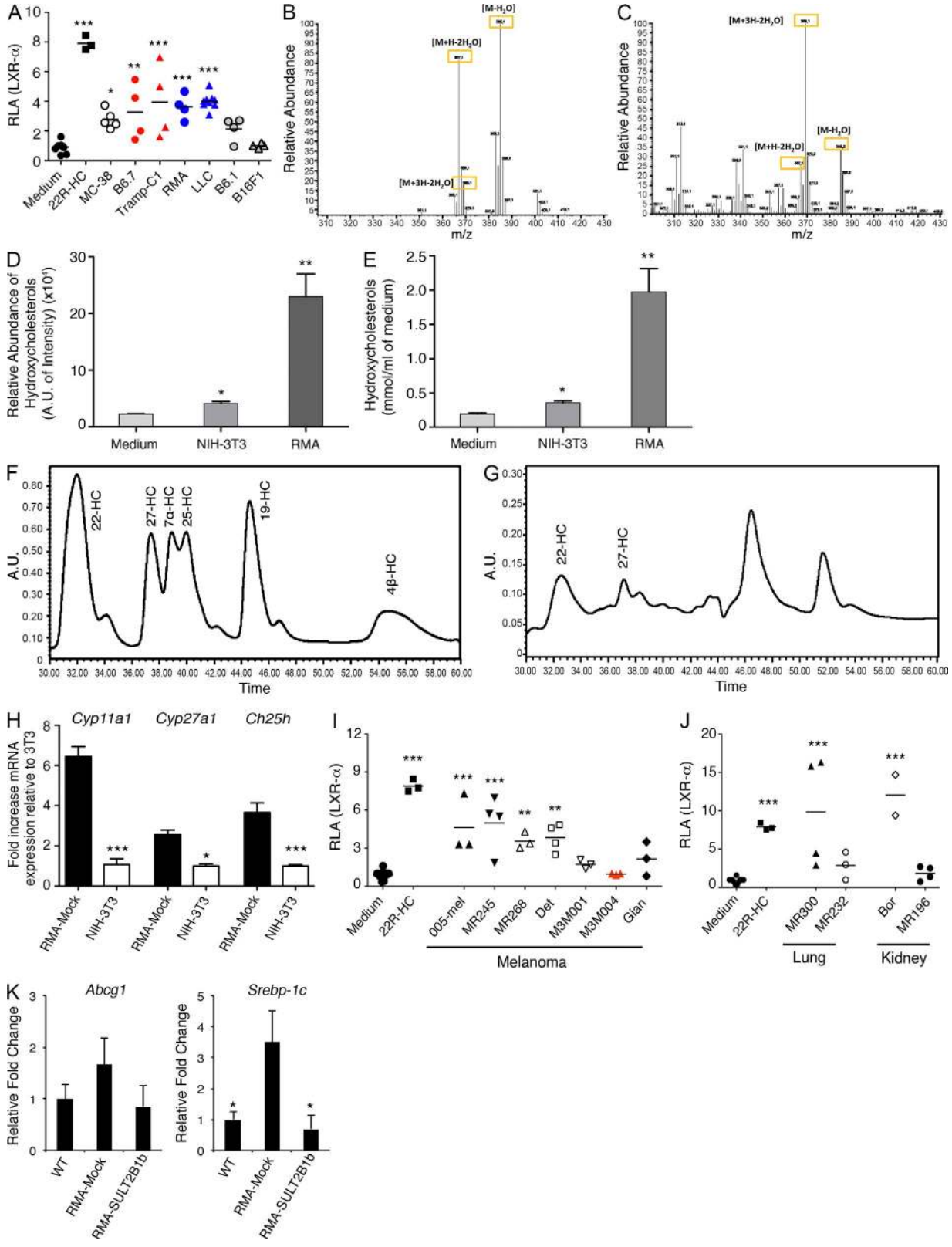

Figure 1. Analysis of tumors releasing LXR ligands and quantification of hydroxycholesterols in cell supernatants by chemical ionization–MS and HPLC analysis. (A) Luciferase assay for LXR-α activation by the indicated tumor CM. Each symbol corresponds to a single experiment, and the line represents the mean value (*, $P < 0.05$; **, $P < 0.01$; ***, $P < 0.0001$). RLA, relative luciferase activity. (B) Spectrum derived from 1 mM hydroxycholesterol mix solution (containing 22R, 22S, 25, 27, 19, 7α, and 4β-HC). The molecular mass for the mix of hydroxycholesterols is 402.67 kD. The collision

(Vanneman and Dranoff, 2012). Tumor microenvironment is composed of various cell types, including tumor-associated macrophages endowed with phenotypes and functions of alternatively activated or M2 macrophages (i.e., expressing IL-10, TGF-β, ARG1, and mannose receptor; Mantovani and Sica, 2010), which have been shown to promote tumor initiation/formation through the induction of immune suppression, matrix remodeling, and angiogenesis (Murdoch et al., 2008), and the heterogeneous $CD11b^+Gr1^+$ myeloid cells, also termed myeloid-derived suppressor cells, comprising immature myeloid progenitors for neutrophils, monocytes, and DCs (Gabrilovich and Nagaraj, 2009). $CD11b^+Gr1^+$ myeloid cells are present in the tumor as well as in bone marrow, peripheral blood, and spleen of tumor-bearing mice (Bronte and Zanovello, 2005). In particular, the immature $CD11b^+Gr1^+$ bone marrow–derived cells, as well as the $CD11b^{high}Gr1^{high}$ $Ly6G^+$ neutrophils, have been recognized as playing an important protumorigenic role by promoting neoangiogenesis (Yang et al., 2004) through the release of MMP9 (Nozawa et al., 2006) and Bv8 (Shojaei et al., 2008), thus mediating refractoriness to anti-VEGF therapy (Shojaei et al., 2007a). Neutrophils have also been shown to suppress antitumor immune responses (Fridlender et al., 2009; De Santo et al., 2010).

Several tumor-derived molecules induce immune suppression by affecting tumor-infiltrating immune cells (Vesely et al., 2011). Some of these molecules are intermediate or final products of the cellular metabolism, such as kynurenine, which, alone or together with the depletion of tryptophan, has been reported to promote T cell anergy (Mellor et al., 2003). Similarly, it has been shown that the increased metabolism of L-arginine by myeloid cells can result in the impairment of lymphocyte responses to tumor cells (Bronte and Zanovello, 2005). Other metabolic pathways have recently emerged as protumorigenic. Products of lipid and cholesterol metabolism have been demonstrated to damage the function of DC both in mouse and in human tumor models. As an example, lipid-loaded DCs are not able to effectively stimulate allogeneic T cells or to present tumor-associated antigens as the result of a reduced antigen processing capability (Herber et al., 2010).

Liver X receptor (LXR) ligands, also named oxysterols, are involved in cholesterol homeostasis (Repa and Mangelsdorf, 2000) and in modulating immune responses (Bensinger and Tontonoz, 2008). The oxysterol 7α,25-HC, which is unable to activate LXRs, has recently been involved in B cell migration to follicles of lymphoid organ through the engagement of EBI2 receptor (Hannedouche et al., 2011; Liu et al., 2011). We have recently shown that LXR ligands/oxysterols are released by cancer cells and inhibit CCR7 expression on maturing DCs, therefore dampening DC migration to draining lymph nodes and antitumor immune responses (Villablanca et al., 2010). Indeed, tumor cells engineered to express the oxysterol inactivating enzyme sulfotransferase 2B1b (SULT2B1b; Fuda et al., 2007), fail to activate LXRs in vitro and are delayed or rejected when infused in immunocompetent mice (Villablanca et al., 2010). Whether tumor-derived LXR ligands/oxysterols are endowed with other protumorigenic functions, thus favoring the formation of hostile microenvironments for immune cells, remains elusive.

Here, we show that tumor-derived oxysterols contribute to recruit neutrophils in a CXCR2-dependent manner within tumor microenvironment, thus favoring neoangiogenesis and/or immunosuppression and tumor growth. Importantly, we show that oxysterol inactivation, as well as CXCR2 inactivation, controls tumor growth, thus identifying a new protumor role of oxysterols and a new therapeutic target for cancer patients.

RESULTS

Functional inactivation of tumor-derived LXR ligands/oxysterols associates with lower levels of $CD11b^{high}Gr1^{high}$ myeloid cells infiltrating tumors

Several mouse tumors release LXR ligands, as evaluated by a luciferase-based assay measuring LXR activation (Fig. 1 A). However, the species of LXR ligands produced by these tumors, as well as their possible effects on tumor-infiltrating immune cells other than DCs (Villablanca et al., 2010), are not known.

To identify the hydroxycholesterol species released by tumor cells, we performed solid-phase extraction of conditioned medium (CM) from the T cell lymphoma RMA and NIH-3T3 cells, the latter being unable to activate LXR (unpublished data), followed by mass spectrometry (MS) analysis. Cholesterol oxidation products share a common fragmentation pattern

product ion pathway is constituted by the following fragment ions: m/z 385 [M-H_2O], m/z 367 [M+H-$2H_2O$], and m/z 369 [M+3H-$2H_2O$]. Results are representative of one out of three experiments. (C) Spectra derived from RMA hydroxycholesterols extract. The same molecular ions m/z 385, m/z 369, and m/z 367 were detected as in B. Results are representative of one out of three experiments. (D) The relative abundance of the three main fragmentation ions (m/z 385, m/z 369, and m/z 367) is expressed as arbitrary intensity units (A.U.) with respect to 1 mM mix solution of hydroxycholesterols. (E) The concentration of hydroxycholesterols with respect to ml of media (µmol/ml) is reported. Results (D and E) are representative of three different experiments (mean ± SEM). *, $P < 0.05$ versus medium; **, $P < 0.01$ versus NIH-3T3–CM. (F and G) HPLC chromatograms of seven single hydroxycholesterol standards (F) and of hydroxycholesterols from RMA-CM (G). Two main hydroxysterols are identified on the basis of the retention time: the 22-HC and 27-HC in a ratio of 4:1. (H) qRT-PCR for *Cyp11a1*, *Cyp27a1*, and *Ch25h* transcripts expression in RMA relative to NIH-3T3. Results are representative of two experiments (mean ± SEM). *, $P < 0.05$; ***, $P < 0.0001$. (I and J) CM from human melanomas (I), and lung and kidney (J) tumors after a few in vitro passages (3–4 passages) were collected and tested for the presence of LXR ligands by LXR luciferase-based reporter assay. Each symbol corresponds to a single tumor CM tested and the line represents the mean value. **, $P < 0.01$; ***, $P < 0.0001$. (K) qRT-PCR analysis for *Abcg1* and *Srebp-1c* mRNA expression in myeloid cells from bone marrow of wild-type (WT), RMA-Mock–, and RMA-SULT2B1b–bearing mice ($n = 3$; mean ± SEM). *, $P < 0.05$. Results are representative of three independent experiments.

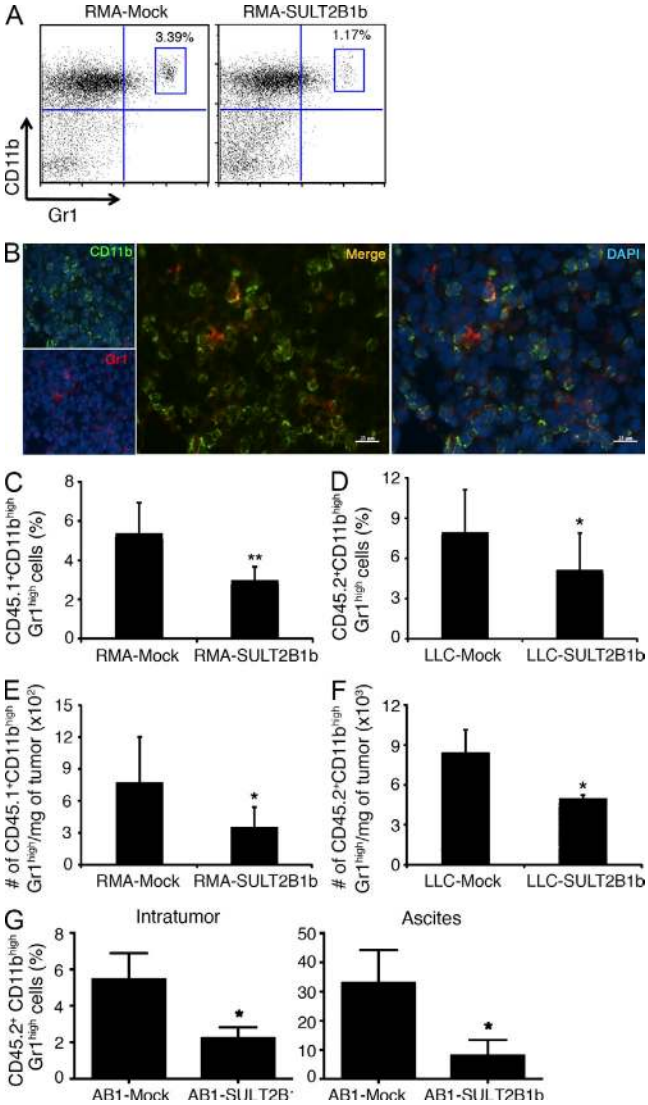

Figure 2. Tumors producing LXR ligands accumulate higher percentages of CD11b^{high}Gr1^{high} myeloid cells at the tumor site. (A and B) Analysis of CD11b^{high}Gr1^{high} cells infiltrating RMA-Mock and RMA-SULT2B1b. (A) Flow cytometry representative of one out of 11–12 experiments. (B) Immunofluorescence of RMA-Mock tumor stained with anti-CD11b (green) and anti-Gr1 (red) mAbs and DAPI (blue). One experiment out of four is shown. Bars, 25 µm. (C and D) Percentage of CD11b^{high}Gr1^{high} cells infiltrating RMA-Mock (n = 12; mean ± SEM) and RMA-SULT2B1b (n = 11; mean ± SEM) tumors (C), and LLC-Mock and LLC-SULT2B1b tumors (n = 13; mean ± SEM; D). *, $P < 0.05$; **, $P = 0.001$. (E and F) Number of CD11b^{high}Gr1^{high} cells/mg of RMA-Mock (n = 12; mean ± SEM) or RMA-SULT2B1b (n = 11) tumors (E), and LLC-Mock and LLC-SULT2B1b (n = 3; mean ± SEM) tumors (F). *, $P < 0.05$. (G) Percentage of CD11b^{high}Gr1^{high} cells infiltrating AB1-Mock and AB1-SULT2B1b tumors (n = 14, Intratumor; n = 8, Ascites; mean ± SEM). *, $P < 0.05$. Results are representative of one (F), two (G), or three (C–E) experiments.

during MS chemical ionization, as reported at http://www.lipidmaps.org. The analysis of hydroxycholesterol extracts from control medium or from NIH-3T3 and RMA-CM showed the same qualitative fragmentation pattern (Fig. 1, B and C), in agreement with the presence of hydroxycholesterols in the fetal calf serum used to supplement the culture media (Pie and Seillan, 1992). Nevertheless, we observed a higher content of hydroxycholesterols in RMA-CM than in culture medium and in NIH-3T3-CM (10- and 5.5-fold, respectively). In particular, the concentrations of hydroxycholesterols, reported as relative abundance of the three molecular ions (m/z 385, 369, and 367), using 1 mM hydroxycholesterol mixture as a standard (Fig. 1 D), were 0.195 ± 0.012 µmol/ml, 0.357 ± 0.027 µmol/ml, and 1.973 ± 0.34 µmol/ml for culture medium, NIH-3T3, and RMA, respectively (Fig. 1 E). Two main hydroxycholesterols could be identified on the basis of the retention time determined by HPLC analysis using a series of standards (Fig. 1 F): 22-HC (22-hydroxycholesterol) and 27-HC in a ratio of 4:1 (Fig. 1 G). Accordingly, we found that RMA cells expressed transcripts for *Cyp11a*, *Cyp27a1*, and *Ch25h* enzymes, which are involved in the synthesis of 22R-HC, 27-HC, and 25-HC, respectively (Björkhem, 2002; Murphy and Johnson, 2008; Mast et al., 2011; Fig. 1 H). In similar experiments, we detected 24S-HC in the Lewis lung carcinoma (LLC)–CM, and the expression of *Cyp46a1* transcript by LLC cells (unpublished data). Moreover, we detected LXR ligands/oxysterols in tumor-CM from some freshly isolated human tumor cells (Fig. 1, I and J). In particular, we detected the oxysterols 22-HC and 24S-HC in CM from 005-mel and MR300 tumor cells (unpublished data). Notably, we detected in vivo a signature of LXR activation (*Abcg1* and *Srebp-1c* up-regulation) in cells of the myeloid compartment purified from the bone marrow of RMA-bearing mice, but not from mice bearing RMA-SULT2B1b tumors, which are unable to produce active LXR ligands/oxysterols (Fig. 1 K). These experiments indicate that tumors may release amounts of oxysterols sufficient to reach and activate LXR-sensitive cells located in organs far away from the tumor.

To evaluate whether these oxysterols were affecting other immune cells besides DCs in the tumor microenvironment, we analyzed by FACS tumor-infiltrating immune cells from 14-d established RMA mock-transduced (RMA-Mock) and RMA-SULT2B1b and found a higher percentage and number of CD11b^{high}Gr1^{high} cells infiltrating RMA-Mock tumors (Fig. 2, A–C and E). We found a similar difference in terms of CD11b^{high}Gr1^{high} cells when comparing mock-transduced LLC (LLC-Mock) with LLC-SULT2B1b (Fig. 2, D and F), and the LXR ligand-releasing AB1-Mock with AB1-SULT2B1b mesotheliomas grown orthotopically in the peritoneal cavity (Fig. 2 G and not depicted).

CD11b^{high}Gr1^{high} cells are continuously recruited to tumor sites

To understand whether the accumulation of these cells was a result of local proliferation or of their continuous recruitment from circulation, we performed parabiosis experiments, joining CD45.1$^+$ and CD45.2$^+$ mice by surgery to establish common blood circulation (Wright et al., 2001; Fig. 3 A). 7 d after RMA challenge in CD45.2$^+$ mice, we separated the mice and analyzed tumor infiltrating cell chimerism by FACS (Fig. 3 A). As early as 2 d after separation, we observed a nearly

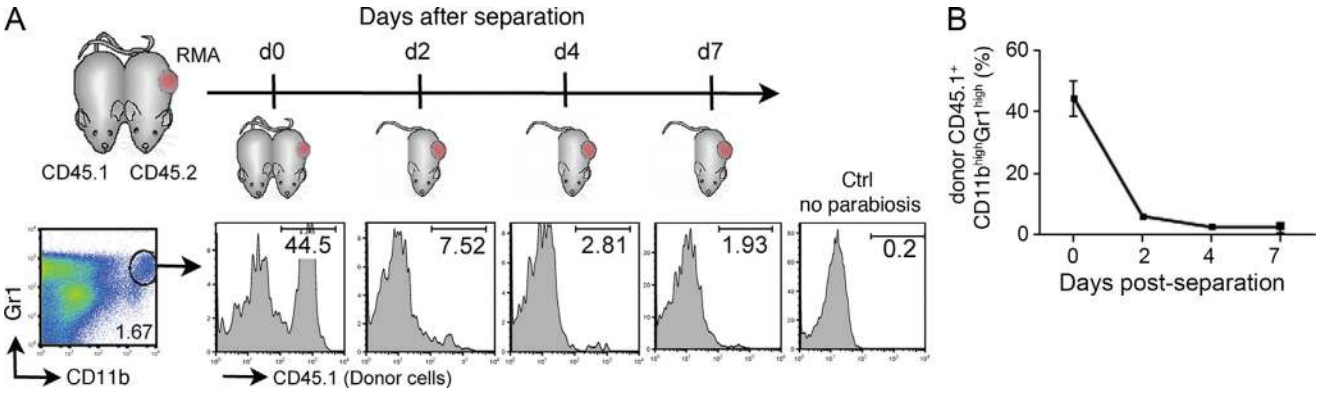

Figure 3. Recruitment of CD11b^{high}Gr1^{high} myeloid cells within LXR ligand–releasing tumors. (A and B) Parabiosis experiments. CD11b^{high}Gr1^{high} gated cells were analyzed for CD45.1 marker at day 0, 2, 4, and 7 after mice separation. A representative FACS analysis of three experiments is shown (A). (B) Quantification of the FACS analysis as in A performed on three mice per group (n = 3 mice per group; mean ± SEM).

complete disappearance of donor CD45.1$^+$CD11b^{high}Gr1^{high} cells (Fig. 3, A and B), thus indicating that these cells are continuously recruited to the tumor site. These results suggest that LXR ligands may behave as chemoattractants for CD11b^{high}Gr1^{high} myeloid cells.

Tumor-derived and naturally occurring LXR ligands are chemotactic factors for CD11b^{high}Gr1^{high} cells in vitro and in vivo

We speculate that CD11b^{high}Gr1^{high} myeloid cells have a BM origin. Hence, we evaluated whether LXR ligands indeed attract BM cells by performing in vitro migration assays. Total BM cells from naive mice migrated to the LXR ligand 22R-HC but not to the inactive isomer 22S-HC (Fig. 4 A). To identify the migrating subset of BM cells, we purified and tested the CD11b$^+$ and CD11b$^-$ populations. Migratory cells were in the CD11b$^+$ cell fraction (Fig. 4 B and not depicted). We observed by FACS analysis that nonmigrating cells co-expressed CD11b and Gr1 markers at intermediate levels (CD11b$^+$Gr1$^+$ cells), whereas migrating cells were CD11b^{high}Gr1^{high} (Fig. S1 A), resembling the cell population detected in vivo within the tumors (Fig. 2 A). Among the other oxysterols tested, 24S-HC, 27-HC, 19-HC, and 25-HC also induced cell migration (Fig. 4 C). On the contrary, cholesterol, some sterol-derived nuclear receptor ligands, and the synthetic LXR ligand T0901317 (T1317) were unable to induce cell migration (Fig. 4, C and D).

To prove that tumor-derived LXR ligands were involved in the migration of CD11b^{high}Gr1^{high} cells in vivo, we injected total BM cells previously labeled with the fluorescent dye CFSE (CFSE$^+$CD45.2$^+$) in NOD-SCID mice bearing RMA-Mock or RMA-SULT2B1b. 18 h later, we analyzed tumors for the presence of injected cells (CFSE$^+$) and found a higher percentage and number of exogenous (CFSE$^+$CD45.2$^+$) CD11b^{high}Gr1^{high} cells infiltrating RMA-Mock, as compared with RMA-SULT2B1b tumors (Fig. 4, F and G, bottom). As expected, the endogenous (CD45.1$^+$) CD11b^{high} Gr1^{high} cells were also more abundant in RMA-Mock (Fig. 4, E and G, top).

Migration of CD11b^{high}Gr1^{high} bona fide neutrophils toward oxysterols is mediated by G protein–coupled receptors (GPCRs) and does not require LXR signaling

To characterize the population of myeloid cells migrating to 22R-HC, we took advantage of the in vitro migration assay. Thus, we compared phenotype and morphology of BM-derived migrating (CD11b^{high}Gr1^{high}) and nonmigrating (CD11b$^+$Gr1$^+$) cells, collected from the lower and upper chamber of migration transwells, respectively (Fig. S1 A). Morphological and cytochemical analyses of the migrating cells showed the presence of nuclei similar to immature granulocytes and mature neutrophils (Fridlender et al., 2009; unpublished data). FACS analysis showed that these cells express Ly6G$^+$ and Ly6b$^+$ markers typical of immature/mature neutrophils (Fig. S1 B), whereas nonmigrating CD11b$^+$Gr1$^+$ cells were phenotypically different (Fig. S1 C). Additionally, CD11b^{high}Gr1^{high} cells expressed higher levels of CCR1, CXCR4, and CXCR2 chemokine receptors than CD11b$^+$Gr1$^+$ cells, as expected for neutrophils (Fig. S1, B and C). In agreement, neutrophils purified from bone marrow by standard methods (Corada et al., 2005) migrated to synthetic and tumor-derived LXR ligands in vitro and in vivo (unpublished data).

As the synthetic LXR ligand T1317 was not capable of triggering cell migration in vitro (Fig. 4 C), we asked whether LXR signaling was, indeed, involved in this migration. CD11b^{high}Gr1^{high}Ly6G$^+$ cells from *Lxr*$\alpha^{-/-}$, $\beta^{-/-}$, and $\alpha\beta^{-/-}$ mice (Alberti et al., 2001) migrated to 22R-HC as well as wild-type cells, indicating that LXR signaling is not required for their migration (Fig. 5 A). The prototypic receptors involved in leukocyte migration belong to the GPCR superfamily (Rossi and Zlotnik, 2000) and can be inhibited by pertussis toxin (PTX). PTX inhibited the migration of CD11b^{high}Gr1^{high}Ly6G$^+$ cells to 22R-HC, thus demonstrating that a GPCR is responsible for the migration of these cells toward LXR ligands (Fig. 5 B).

Migration of neutrophils toward 22R-HC in vitro and in vivo requires CXCR2 engagement and signaling

The recruitment of CD11b^{high}Gr1^{high}Ly6G$^+$ cells (hereafter referred to as BM-derived neutrophils) into tumors could be

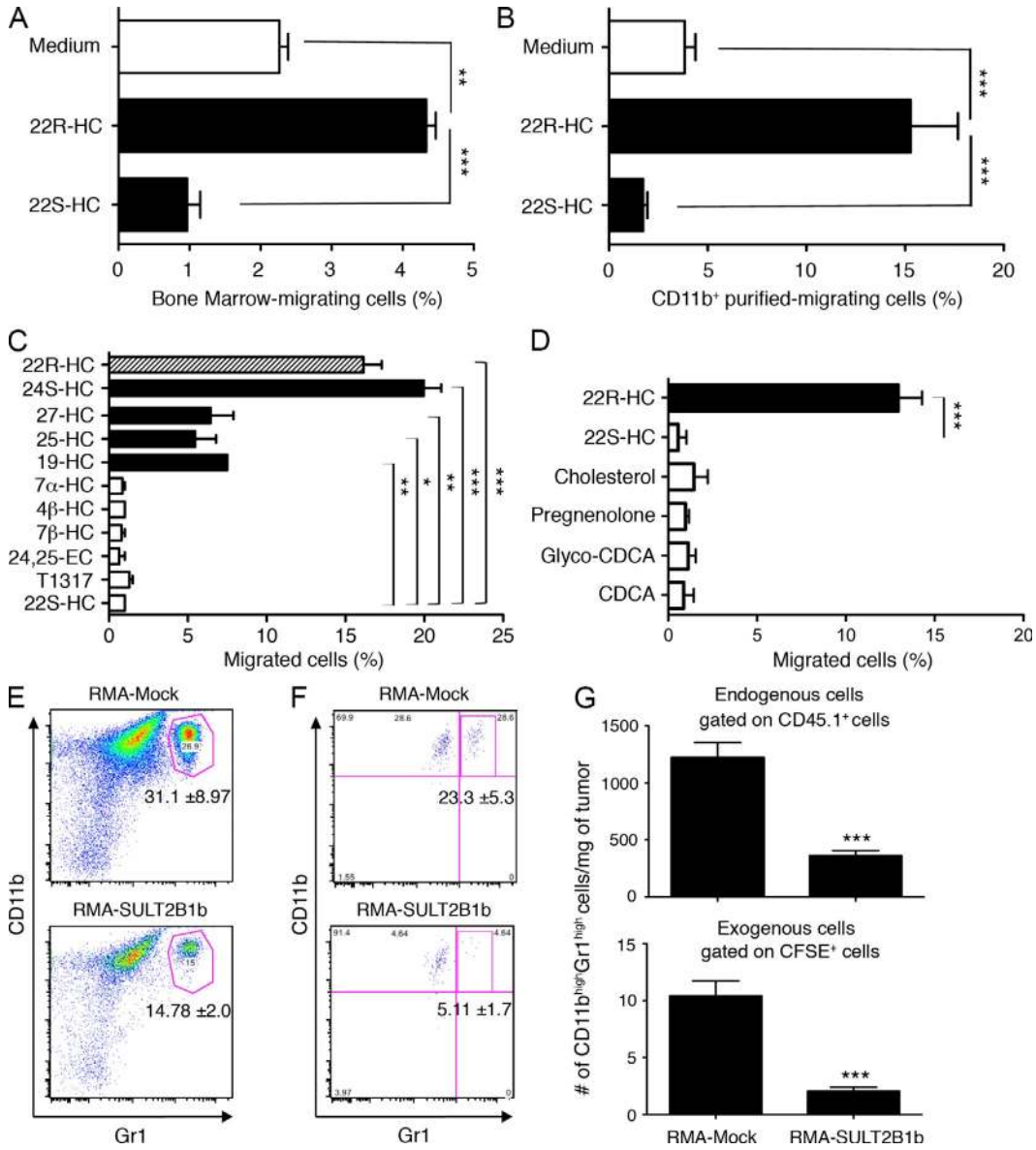

Figure 4. In vitro and in vivo migration of BM-derived CD11b^{high}Gr1^{high} myeloid cells toward natural and tumor-released LXR ligands. (A and B) In vitro migration of total BM cells (A) and CD11b$^+$ purified cells (B) toward 15 µM of the LXR ligands 22R-HC and 22S-HC (mean ± SEM). Results are representative of four experiments. **, P < 0.01; ***, P < 0.0001. (C and D) Migration of purified CD11b$^+$Gr1$^+$ cells to LXR ligands and to other sterol-derived compounds. (C) 22R-HC, 24S-HC, 27-HC, 19-HC, 25-HC, 7α-HC, 4β-HC, 7β-OH, 24,25 EpoxyChol, T1317, and 22S-HC ligands were tested at 15 µM. Because of toxicity, 7α-HC and 24,25-EC were tested at 5 µM, whereas 19-HC was tested at 1 µM (mean ± SEM). Results are representative of two experiments. *, P < 0.05; **, P < 0.01; ***, P < 0.0001. (D) CDCA, chenodeoxycholic acid; GlycoCDCA, glycine chenodeoxycholic acid. CDCA and glycoCDCA are FXR ligands, and pregnenolone is an SXR ligand (mean ± SEM). Results are representative of three experiments. ***, P < 0.0001. (E and F) FACS analysis of endogenous CD45.1$^+$CD11b^{high}Gr1^{high} (E) and exogenous CFSE$^+$CD11b^{high}Gr1^{high} (F) cells infiltrating RMA-Mock and RMA-SULT2B1b tumors after i.v. infusion of CFSE$^+$ BM cells. One of out of five experiments is shown. Numbers in the plots represent mean ± SEM of the percentages of endogenous and exogenous cells (n = 5). (G) Number of endogenous CD45.1$^+$CD11b^{high}Gr1^{high} and exogenous CFSE$^+$CD11b^{high}Gr1^{high} cells infiltrating RMA-Mock and RMA-SULT2B1b tumors (n = 5; mean ± SEM). Results are representative of five mice per group. ***, P = 0.0003.

mediated by the CXCL12–CXCR4 and CXCL5–CXCR2 axes (Yang et al., 2008). We therefore performed a migration assay toward 22R-HC, CXCL5, CXCL12, and CCL3, a ligand of CCR1. BM-derived neutrophils migrated to 22R-HC, CXCL5, and SDF-1α, whereas migration to MIP-1α was negligible (Fig. 5 C). In addition, the pretreatment of BM-derived neutrophils with 22R-HC induced the heterologous desensitization of the cells to the subsequent response to CXCL5 but did not affect the migration to CXCL12 (Fig. 5 C). These results suggest that 22R-HC and CXCL5 may share the same chemotactic receptor, namely CXCR2. Accordingly, heterologous desensitization of BM-derived neutrophils with CXCL5

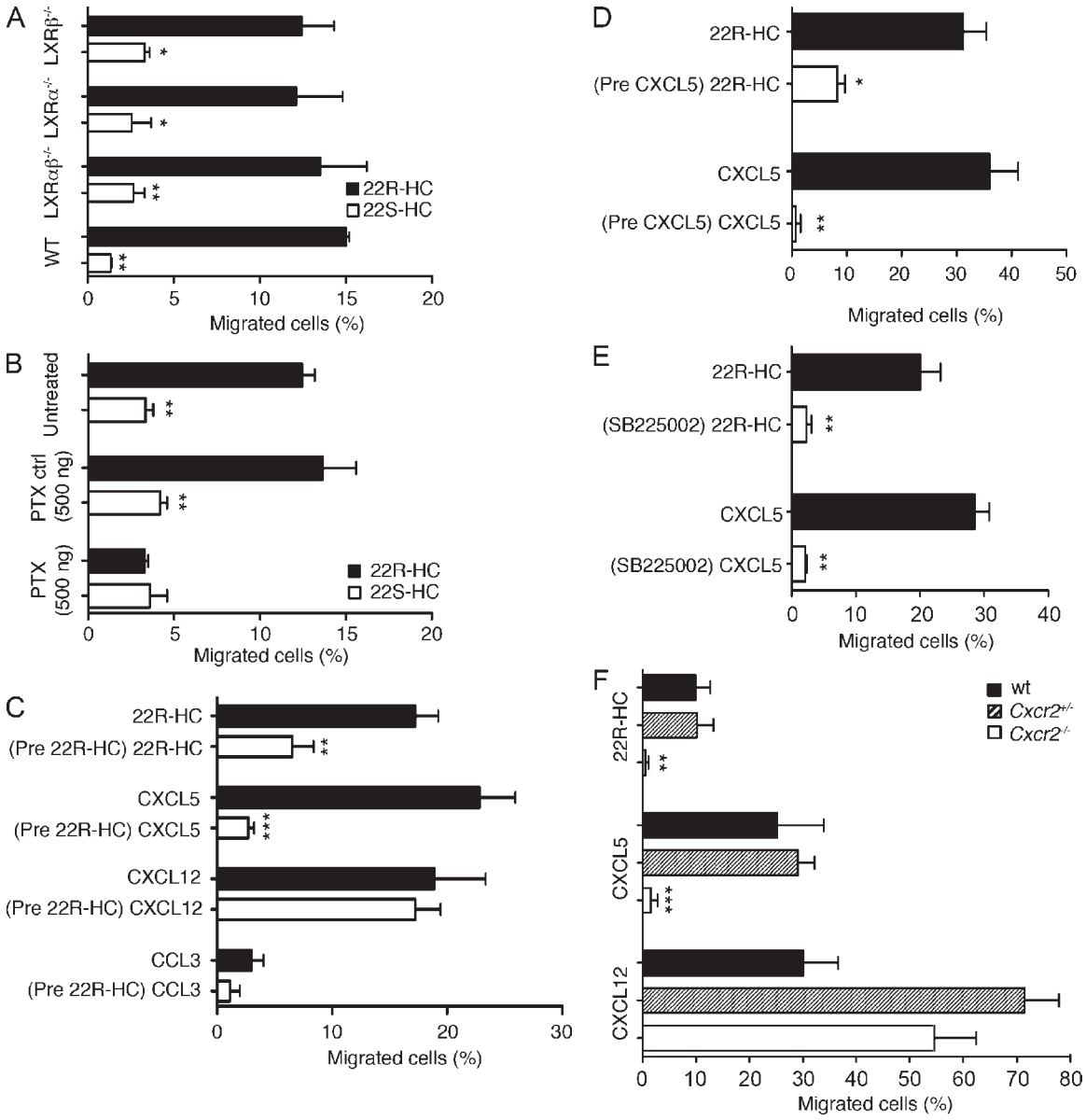

Figure 5. Migration of CD11b^{high}Gr1^{high} neutrophils toward LXR ligands is independent of LXR and mediated by the GPCR CXCR2. (A) In vitro migration of CD11b$^+$Gr1$^+$ cells from wild-type (WT) and *Lxr*s-deficient mice to 15 µM 22R-HC or 22S-HC (mean ± SEM). Results are representative of two experiments. *, $P < 0.05$; **, $P < 0.01$. (B) Migration of PTX-treated CD11b$^+$Gr1$^+$ cells to 15 µM 22R-HC or 22HS-HC (mean ± SEM). Results are representative of two experiments. **, $P < 0.01$. (C) Migration of pretreated CD11b$^+$Gr1$^+$ cells to 15 µM 22R-HC, or 100 ng CXCL5, CXCL12, or CCL3 (mean ± SEM). Results are representative of four experiments. **, $P < 0.01$; ***, $P < 0.0005$. (D and E) Migration of CXCL5 (E) or SB225002 (F) pretreated CD11b$^+$Gr1$^+$ cells to 15 µM 22R-HC or 100 ng CXCL5 (mean ± SEM). Results are representative of two experiments. *, $P < 0.05$; **, $P < 0.01$. (F) Migration of WT, *Cxcr2*$^{+/-}$, and *Cxcr2*$^{-/-}$ CD11b$^+$Gr1$^+$ cells to 15 µM 22R-HC, or 100 ng CXCL5 or CXCL12 (mean ± SEM). Results are representative of four experiments. **, $P < 0.01$; ***, $P < 0.0001$.

or their treatment with the CXCR2 antagonist SB225002 (White et al., 1998) inhibited their migration to CXCL5 and to 22R-HC (Fig. 5, D and E). To finally prove the role of the CXCR2 receptor, we performed migration experiments using BM-derived neutrophils from *Cxcr2*$^{-/-}$ mice (Cacalano et al., 1994). These cells did not migrate to either CXCL5 or 22R-HC, whereas they migrated to SDF-1α, demonstrating that CXCR2 is indeed the receptor involved in the migration of BM-derived neutrophils toward 22R-HC (Fig. 5 F).

To investigate the role of the oxysterol–CXCR2 axis in neutrophil recruitment in vivo, we performed matrigel plug experiments. To distinguish neutrophil migration induced by 22R-HC from that induced by other CXCR2-binding chemokines that are locally released during the inflammation induced by matrigel inoculation, we injected mice with matrigel

plugs containing CXCL5, 22R-HC, or 22S-HC alone or in the presence of anti-CXCL1, 3, 5, and 7 mAbs (Fig. 6 A). 5 h later, plugs were analyzed for the presence of $CD11b^+Ly6G^+$ neutrophils (Fig. 6 A). CXCL5 and 22R-HC induced a high recruitment of neutrophils, whereas 22S-HC behaved as matrigel alone (Fig. 6 A). Anti-CXCL mAbs almost completely inhibited migration induced by CXCL5 (88.6% inhibition) and 22S-HC (80% inhibition), whereas 22R-HC–induced migration was only partly inhibited (48.3% inhibition) (Fig. 6 A), indicating that 22R-HC is indeed able to recruit neutrophils in vivo. Accordingly, the percentage of neutrophil infiltration in RMA-Mock and RMA-SULT2B1b (Fig. 2 C) correlated with the availability of active oxysterols, but not with the content of CXCL1 and CXCL5 chemokines detected within the tumor, as shown by quantitative analyses reporting higher levels of CXCL1 and CXCL5 chemokines in RMA-SULT2B1b than in RMA-Mock (Fig. 6, B and C). 22R-HC–induced migration was mediated by CXCR2, as it was inhibited when mice bearing 22R-HC–embedded plugs were treated with the CXCR2 antagonist SB225002 (Fig. 6 D). Finally, in vivo neutrophil migration was also independent of LXR signaling, as demonstrated by the migration of $Lxr\alpha\beta^{-/-}$ neutrophils toward 22R-HC–embedded matrigel plugs (Fig. 6 E).

The engagement and activation of CXCR2 by 22R-HC was demonstrated by three experimental approaches. First, 22R-HC was able to induce CXCR2 down-regulation, as evaluated by FACS analysis (Fig. 7 A). Second, in a concentration-dependent manner, 22R-HC stimulated the binding of ^{35}S-GTPγS to membranes from CXCR2-expressing L1.2 cells, but not from Mock-L1.2 cells, with an EC_{50} value of 1.32 ± 0.25 μM (Fig. 7, B and C). On the contrary, 22S-HC did not activate any ^{35}S-GTPγS binding, suggesting that this oxysterol does not interact with CXCR2 (Fig. 7, B and C). As expected, the natural CXCR2 ligand IL-8 stimulated ^{35}S-GTPγS binding, with an EC_{50} of 2.50 ± 0.17 nM (Fig. 7 B). Furthermore, we observed a dose-dependent inhibition of ^{35}S-GTPγS binding when 22R-HC was displaced by increasing concentrations of the CXCR2 antagonist SB225002 (Fig. 7 D). Third, 22R-HC inhibited the cAMP formation elicited by 1 μM forskolin in a dose-dependent manner, with an EC_{50} value of 1.32 ± 0.25 μM in CXCR2-expressing CHOK1 but not in Mock-CHOK1 cells (Fig. 7, D and E). Yet in this system, the CXCR2 antagonist SB225002 counteracted the inhibition of cAMP formation elicited by 10 μM 22R-HC in a dose-dependent manner (unpublished data). Notably, the EC_{50} values of 22R-HC–CXCR2 interactions that we detected (1.32 μM) are in the same range as those reported for 22R-HC–LXR activation (1.5 μM; Janowski et al., 1996), indicating that 22R-HC oxysterol is able to activate both LXRs and CXCR2 with a similar potency.

Additionally, 22R-HC and 25-HC displaced ^{125}I-IL-8 from CXCR2-expressing cells in a dose-dependent manner (Fig. 7 G), whereas 22S-HC and 4β-HC (two oxysterols unable to promote cell migration, Fig. 4 C) did not (unpublished data), thus suggesting that 22R-HC, 25-HC and IL-8 could bind the same domain of CXCR2.

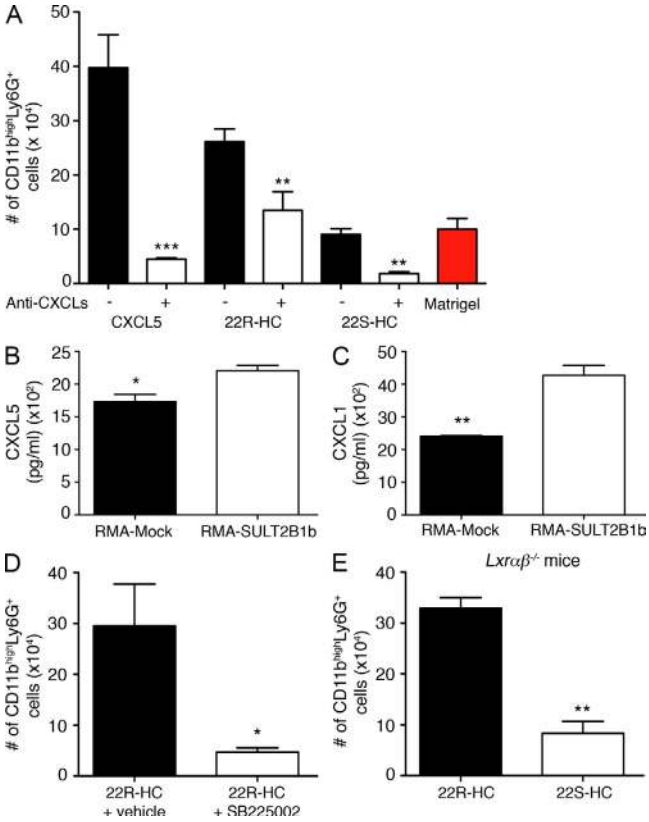

Figure 6. In vivo migration of neutrophils toward 22R-HC Oxysterol. (A) Total number of $CD11b^{high}Ly6G^+$ neutrophils migrated toward matrigel plugs embedded with 500 ng CXCL5, or 500 μM 22R-HC or 22S-HC in the absence (black bars) or presence (white bars) of mAbs blocking CXCL1, 3, 5, and 7 chemokines. Neutrophil migration toward matrigel alone is represented in red. Results are representative of three to six mice per group (mean ± SEM). **, $P < 0.01$; ***, $P < 0.0001$. (B and C) Quantification of tumor environment–produced CXCL1 and CXCL5 chemokines. Cell suspensions from 7-d established RMA-SULT2B1b tumors release higher amounts of CXCL5 (B) and CXCL1 (C) chemokines than cell suspensions from 7-d established RMA-Mock (mean ± SEM). Data are representative of three experiments. *, $P < 0.05$; **, $P < 0.01$. (D) Total number of $CD11b^{high}Ly6G^+$ neutrophils migrated toward matrigel plugs embedded with 500 μM of 22R-HC after the treatment of mice with the CXCR2 antagonist SB225002 (white bars) or vehicle (black bars; $n = 6$ mice; mean ± SEM). Results are representative of two experiments. *, $P < 0.05$. (E) Total number of $Lxr\alpha\beta^{-/-}$ $CD11b^{high}Ly6G^+$ neutrophils infiltrating matrigel plugs embedded with 500 μM 22R-HC or 22S-HC. Results are representative of three mice per group (mean ± SEM). **, $P = 0.0015$.

Oxysterol-migrating neutrophils favor tumor growth by promoting neoangiogenesis or immunosuppression

Because the inactivation of oxysterols by SULT2B1b-expressing tumors induces tumor growth delay or rejection (Villablanca et al., 2010), we hypothesized that neutrophils recruited by tumor-derived oxysterols could exert protumor activities (i.e., immunosuppression and/or neoangiogenesis), as already reported by others (Yang et al., 2004; Nozawa et al., 2006; Fridlender et al., 2009). Therefore, we investigated the protumor functions of 22R-HC–migrating

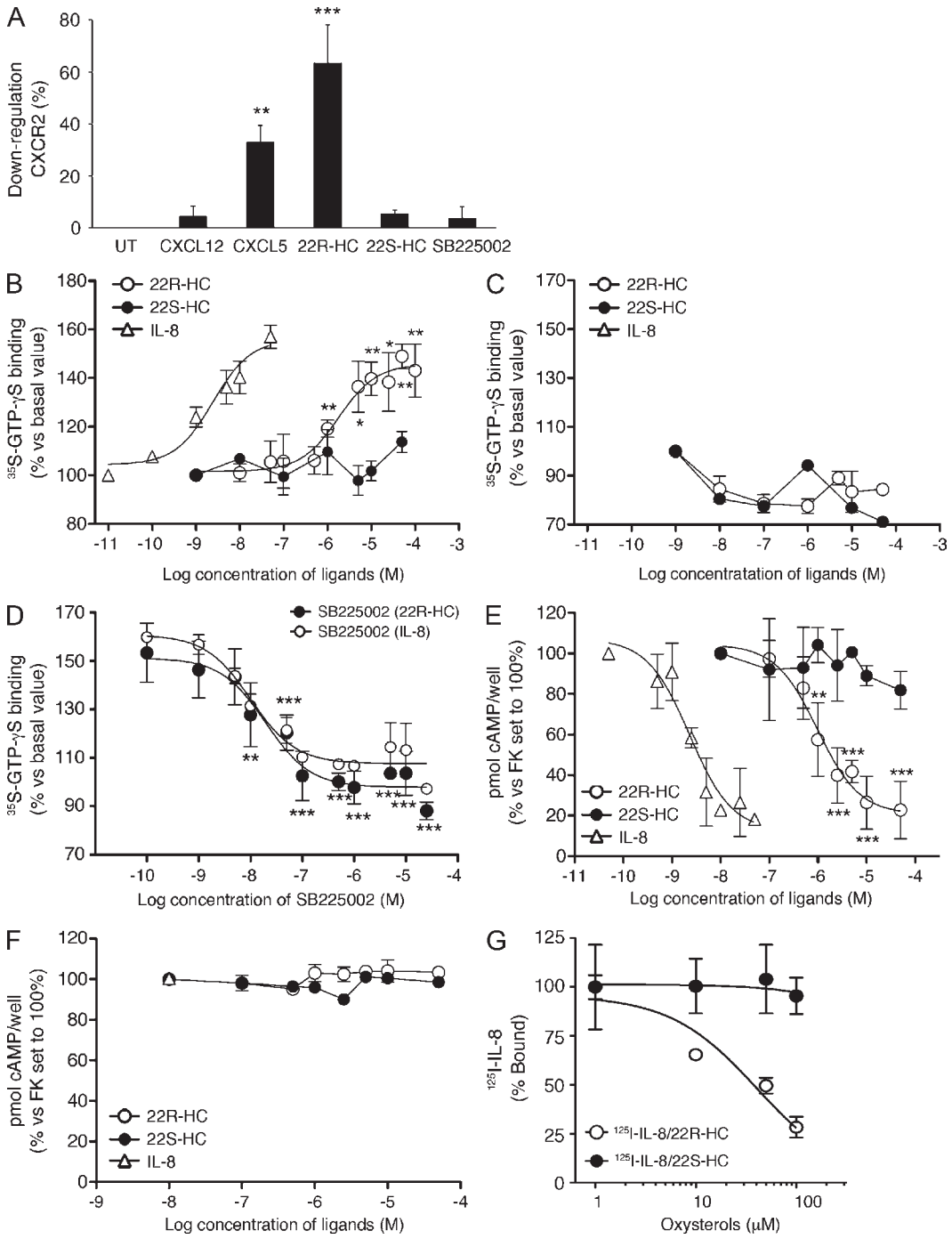

Figure 7. The Oxysterol 22R-HC binds and activates CXCR2. (A) Flow cytometric analysis of CXCR2 expression by CD11b^{high}Gr1^{high} cells untreated (UT) or incubated with CXCL12, CXCL5, 22R-HC, 22S-HC, or SB225002 (mean ± SEM). Results are representative of three experiments. **, $P < 0.01$; ***, $P < 0.0005$. (B and C) Dose-dependent stimulation of ^{35}S-GTPγS binding on L1.2-CXCR2 (B) or L1.2-mock (C) cellular membranes by oxysterols and IL-8. All data are expressed as percentage of basal ^{35}S-GTPγS binding (set to 100%; mean ± SEM). Results are representative of three experiments. *, $P < 0.05$; **, $P < 0.01$ versus basal value. (D) SB225002 inhibits ^{35}S-GTPγS binding stimulated by 10 μM 22R-HC (IC_{50} of 22.41 ± 4.83 nM) and by 10 nM IL-8 used as control (IC_{50} of 16.64 ± 3.64 nM). All data are expressed as percentage of basal ^{35}S-GTPγS binding (set to 100%; mean ± SEM). Results are representative of three experiments. **, $P < 0.01$; ***, $P < 0.001$ versus basal value. (E and F) Dose-dependent inhibition of forskolin-induced cAMP accumulation in CXCR2-expressing cells (E) or mock cells (F) by oxysterols and IL-8. Results are expressed as percentage of FK-stimulated cAMP levels, set to 100% (mean ± SEM). Results are representative of three experiments. **, $P < 0.01$; ***, $P < 0.001$ versus basal value. (G) Percentage of ^{125}I-IL-8 bound to L1.2-CXCR2 cells in the presence of 100, 50, 10, or 1 μM 22R-HC or 22S-HC (mean ± SEM). Results are representative of three experiments.

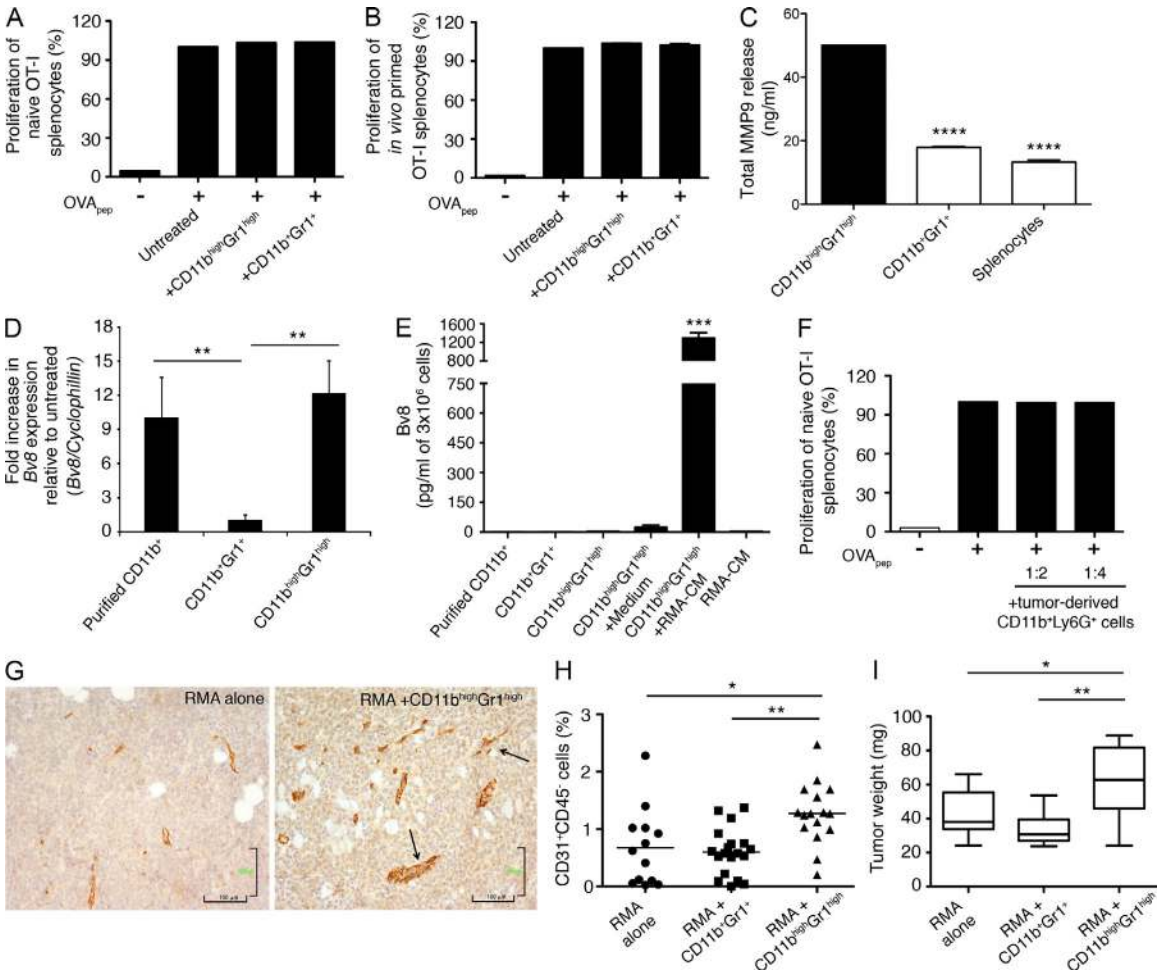

Figure 8. Oxysterol-migrating neutrophils enhance RMA tumor growth by promoting neoangiogenesis. (A and B) Proliferation of OT-I splenocytes naive (A) or memory (B) labeled with the cytosolic dye CFSE and pulsed with the ovalbumin peptide SIINFEKL in the presence of 50% $CD11b^{high}Gr1^{high}$ (22R-HC migrating) or $CD11b^{+}Gr1^{+}$ (22R-HC nonmigrating) cells (mean ± SEM). Results are representative of two experiments. (C) 22R-HC migrating neutrophils release higher amounts of MMP9 than nonmigrating cells and splenocytes (mean ± SEM). Results are representative of two experiments. ****, $P < 0.0001$. (D) qRT-PCR analysis for *Bv8* mRNA expression in $CD11b^{+}$, and 22R-HC migrating ($CD11b^{high}Gr1^{high}$) and nonmigrating ($CD11b^{+}Gr1^{+}$) cells (mean ± SEM). Results are representative of three experiments. **, $P < 0.01$. (E) Release of Bv8 protein by $CD11b^{+}$, and 22R-HC migrating ($CD11b^{high}Gr1^{high}$) and nonmigrating ($CD11b^{+}Gr1^{+}$) cells and by 22R-HC migrating cells incubated with medium or RMA-CM. RMA-CM alone was also tested (mean ± SEM). Results are representative of three experiments. ***, $P < 0.0001$. (F) Proliferation of OT-I naive splenocytes labeled with the cytosolic dye CFSE and pulsed with the SIINFEKL peptide in the presence of 50% (1:2) or 25% (1:4) of $CD11b^{high}Ly6G^{+}$ neutrophils isolated from RMA tumors (mean ± SEM). Results are representative of two experiments. (G) Immunohistochemistry showing $CD31^{+}$ endothelial cells in RMA alone (left) or coinjected with $CD11b^{high}Gr1^{high}$ neutrophils (right). Arrows indicate enlarged and abnormally shaped vessels. One experiment out of four is shown. Bars, 100 µm. (H) Percentage of $CD45^{-}CD31^{+}$ cells (presented as in A). Individual mouse data are shown (mean, horizontal line). *, $P < 0.05$; **, $P < 0.01$. (I) Box plots representing weights of RMA tumors alone ($n = 13$) or coinjected with 22R-HC migrating ($CD11b^{high}Gr1^{high}$; $n = 16$) or nonmigrating ($CD11b^{+}Gr1^{+}$; $n = 19$) cells. Results are representative of three experiments. *, $P < 0.05$; **, $P < 0.01$.

neutrophils in vitro and in vivo in RMA, AB1, and LLC tumor models.

In vitro, BM-derived 22R-HC–migrating neutrophils ($CD11b^{high}Gr1^{high}$) were unable to suppress both the priming (Fig. 8 A) and the restimulation (Fig. 8 B) of OVA-specific OT-I T cells. However, they released a high amount of total MMP-9 (Nozawa et al., 2006; Fig. 8 C), expressed high mRNA levels of the proangiogenic factor *Bv8* (Shojaei et al., 2008; Fig. 8 D), and released Bv8 when exposed for 18 h to tumor CM (Fig. 8 E).

In vivo, we tested whether RMA-infiltrating neutrophils were endowed with immunosuppressive functions, as neutrophils may acquire an immunosuppressive ability within the tumor microenvironment (Fridlender et al., 2009; De Santo et al., 2010). However, we failed to detect any suppression of OT-I T cell activation (Fig. 8 F). In agreement with the reported in vitro proangiogenic functions, we observed an increased number of abnormal $CD31^{+}$ vessels by immunohistochemistry (Fig. 8 G) and a higher percentage of $CD45^{-}CD31^{+}$ cells in 6-d established matrigel plugs

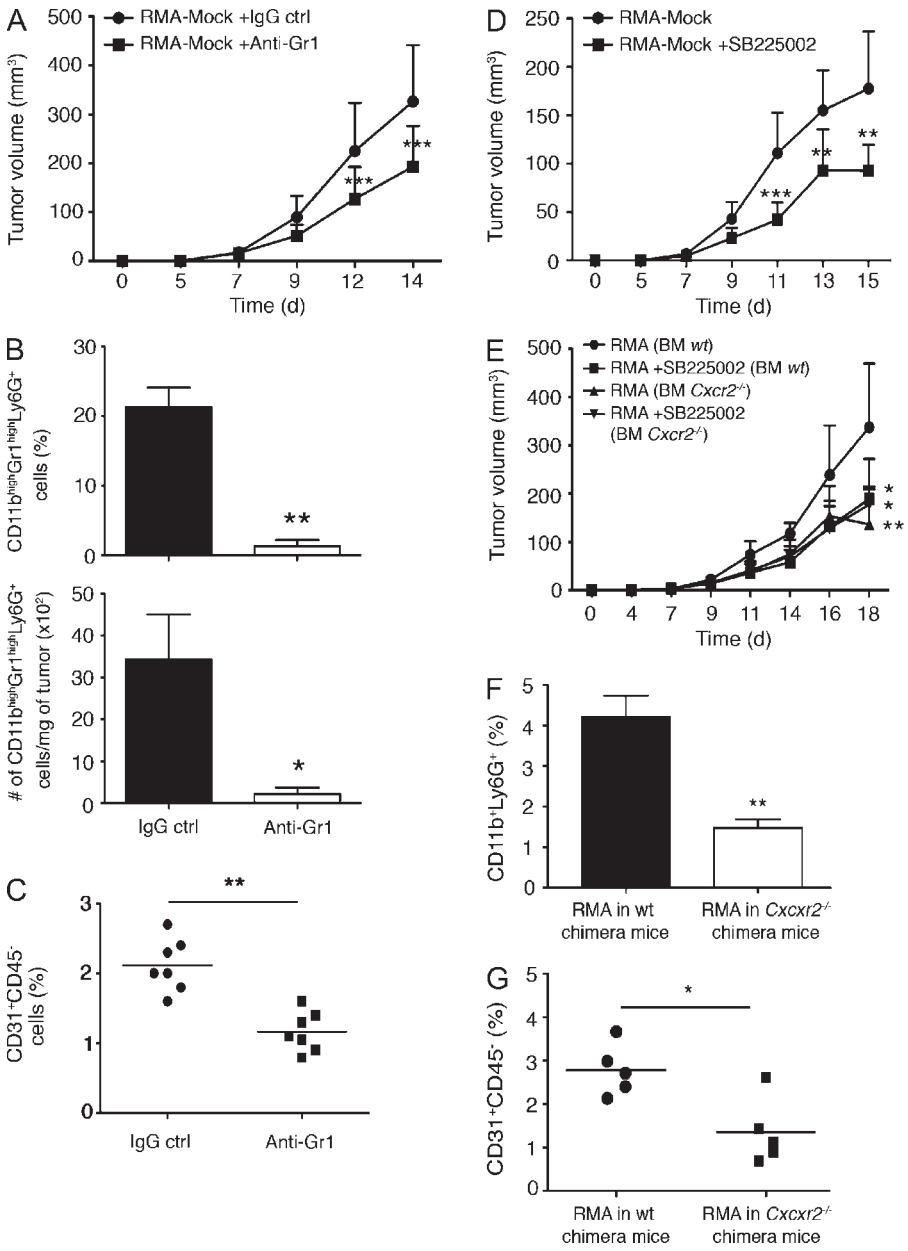

Figure 9. Neutrophil depletion and CXCR2 inactivation control tumor growth by reducing angiogenesis in RMA tumor model. (A) RMA tumor growth in mice administered with 30 µg anti-Gr1 or control antibody (n = 15 mice per group). Results are representative of two experiments. ***, P = 0.0001. (B) Percentage and number of RMA-infiltrating neutrophils after intratumor administration of anti-Gr1 or control antibody (n = 5 mice per group; mean ± SEM). *, P = 0.038; **, P = 0.0033. (C) Percentage of $CD45^{-}CD31^{+}$ cells in RMA injected with anti-Gr1 or control antibody (n = 7 mice per group). Individual mouse data are shown (mean, horizontal line). Results are representative of two experiments. **, P = 0.0031. (D) Treatment of RMA-Mock–bearing mice with vehicle or 0.8 mM SB225002 (n = 7–8; mean ± SEM). Results are representative of one out of two experiments. **, P < 0.001; ***, P = 0.0009. (E) Growth of RMA in WT and *Cxcr2*$^{-/-}$ chimera mice treated or not with 0.8 mM SB225002 (n = 5–6; mean ± SEM). Results are representative of one out of two experiments. *, P < 0.05; **, P = 0.0001. (F) Percentage of $CD11b^{+}Ly6G^{+}$ neutrophils infiltrating RMA-Mock injected in WT (n = 5; mean ± SEM) or in *Cxcr2*$^{-/-}$ (n = 6; mean ± SEM) chimera mice. **, P = 0.0010. (G) Percentage of $CD45^{-}CD31^{+}$ cells in RMA-Mock injected in WT or *Cxcr2*$^{-/-}$ chimera mice (n = 5 mice per group). Individual mouse data are shown (mean, horizontal line). *, P = 0.01.

containing RMA (Fig. 8 H) or B16F1 (not depicted) admixed with 22R-HC–migrating $CD11b^{high}Gr1^{high}$ neutrophils. These results paralleled the increased tumor weight we observed when RMA tumors were admixed with 22R-HC–migrating $CD11b^{high}Gr1^{high}$ neutrophils (Fig. 8 I). In contrast, we observed tumor growth delay, decrease of neutrophil but not of $CD11b^{+}Gr1^{+}$ cell infiltration, and reduction of $CD45^{-}CD31^{+}$ endothelial cells when we treated RMA-bearing mice intratumor with an anti-Gr1 mAb (Fig. 9, A–C; and not depicted).

To investigate the role of CXCR2 receptor activation in vivo and to mimic a possible pharmacologic antitumor therapy, we treated RMA-bearing mice with the CXCR2 antagonist SB225002 and found a significant delay of RMA growth (Fig. 9 D). However, as in the tumor microenvironment, CXCR2 is expressed by neutrophils and at lower levels (unpublished data) by some mature endothelial cells (Strieter et al., 2006), and we performed tumor growth experiments in wild-type and in *Cxcr2*$^{-/-}$ bone marrow chimera to distinguish the role of the two cell populations. SB225002 significantly delayed tumor growth in wild-type but not in *Cxcr2*$^{-/-}$ chimera mice (Fig. 9 E). Moreover, in these tumors we detected a reduced percentage of neutrophils and CD45^{-}CD31^{+} endothelial cells (Fig. 9, F and G), thus demonstrating that in the RMA tumor model, tumor-released oxysterols favor tumor growth by recruiting proangiogenic neutrophils. Whether oxysterols may also have an effect on BM-derived endothelial progenitor cells expressing CXCR2 deserves a deeper investigation in suitable tumor models (Shaked et al., 2008).

As reported above, we also investigated the possible protumor role of oxysterol-recruited neutrophils in AB1 and LLC tumor models. We observed a reduced number of peritoneal tumor nodules associated with a reduction of neutrophils and CD45^{-}CD31^{+} endothelial cells when we treated AB1-bearing mice with the CXCR2 antagonist SB225002 (Fig. 10, A–C). Similar results were obtained by inactivating oxysterols with SULT2B1b. Indeed, we observed a lower number of peritoneal tumor nodules and prolonged survival of mice bearing AB1-SULT2B1b as compared with mice bearing AB1-Mock tumors (not depicted and Fig. 10 D). The prolonged survival was associated with a lower percentage of infiltrating neutrophils (Fig. 2 G) and CD45^{-}CD31^{+} endothelial cells (Fig. 10 E).

In the LLC tumor model, we also observed a significant growth delay when we treated tumor-bearing mice with SB225002 (Fig. 10 F) and when LLC was grown in *Cxcr2*$^{-/-}$ bone marrow chimera mice (Fig. 10 G). In this experimental setting, tumor growth delay paralleled the reduction of neutrophil infiltration (Fig. 10 H). However, we failed to detect any difference in the percentage of CD45^{-}CD31^{+} cells between LLC tumors from wild-type and *Cxcr2*$^{-/-}$ chimera mice (Fig. 10 I). Similar results were obtained when BM-derived neutrophils were coinjected in matrigel admixed with LLC tumor cells (Fig. 10 J). These results suggest that mechanisms different from those acting in the RMA and AB1 tumors are responsible for tumor promotion by neutrophils in LLC tumor, such as immune suppression. Indeed, neutrophils purified from LLC tumors were able to suppress OT-I T cell activation (Fig. 10 K), thus indicating that in this tumor model, neutrophils mainly exert their protumorigenic activity by the immune suppression of antitumor immune responses.

Altogether, these results indicate that some tumor-derived oxysterols recruit neutrophils in a CXCR2-dependent manner, which in turn exploit (i.e., neoangiogenesis) or acquire (i.e., immune suppression) protumor activities, thus favoring tumorigenesis. The inactivation of the oxysterol–CXCR2–neutrophil axis is able to effectively counteract tumor growth.

DISCUSSION

In recent years, bone marrow–derived immature and mature myeloid cells have been extensively investigated, as they are endowed with a high capability to exert protumor functions (Gabrilovich et al., 2012). Indeed, these cells can suppress antigen-specific immune responses (immature myeloid cells or myeloid-derived suppressor cells), exert a proangiogenic activity (immature myeloid cells or neutrophils; Murdoch et al., 2008; Motz and Coukos, 2011), or induce chemoresistance and invasion or metastasis (immature myeloid cells; Yang et al., 2008; Acharyya et al., 2012). These cells are recruited to tumor microenvironment mainly by chemokines constitutively released by tumor and stromal cells (Mantovani et al., 2010; Qian et al., 2011; Acharyya et al., 2012) or produced after some aggressive treatments (Kerbel, 2008). Our study highlights an unanticipated role of tumor-derived oxysterols/LXR ligands, which contribute to the recruitment of protumor neutrophils in a CXCR2-dependent manner, ultimately favoring tumor growth.

The migration of neutrophils to the oxysterol 22R-HC did not require LXR signaling because it occurred also with neutrophils from *Lxr*$\alpha^{-/-}$, $\beta^{-/-}$, and $\alpha\beta^{-/-}$ mice but required the functional interaction with the GPCR CXCR2, as demonstrated by the 22R-HC–mediated activation of ^{35}S-GTPγS binding and by the inhibition of cAMP formation elicited by forskolin stimulation. The interaction between oxysterols and GPCRs has recently been described to occur for the oxysterol 7α,25-HC, which specifically binds EBI2 but not LXRs (Hannedouche et al., 2011). The CXCR2-activating oxysterols identified by our study have been primarily reported to bind LXRs (Janowski et al., 1996). However, the EC_{50} values of CXCR2/22R–HC interaction we measured (1.32 μM) turned out to be very similar to those reported by Janowski et al. (1996) for LXR/22R–HC interaction (1.5 μM). In this context, our results are in agreement with a recent in vitro study showing that the oxysterol 20S-HC activates the 7-transmembrane oncoprotein smoothened, in addition to LXRs, with a similar potency (i.e., $\sim$3 μM for smoothened, and 4–7 μM for LXRα; Nachtergaele et al., 2012). Notably, Nachtergaele et al. (2012) reported that the oxysterol 20S-HC could act as allosteric modulator of protein binding. Instead, in our system we did not observe any synergistic effect when neutrophils were allowed to migrate in vitro toward mixtures of 22R-HC and CXCR2 ligands (unpublished data). Altogether, these observations identify the oxysterols as molecules endowed with a broad range of activity (i.e., binding to LXRs and/or to other receptors) depending on the tissue and the pathophysiologic conditions of the microenvironment in which they are produced. Indeed, in our tumor models, the dual role of oxysterols, i.e., the CXCR2-mediated recruitment of protumorigenic neutrophils and the recently described LXR-dependent dampening of DC migration (Villablanca et al., 2010), coexists and adds up

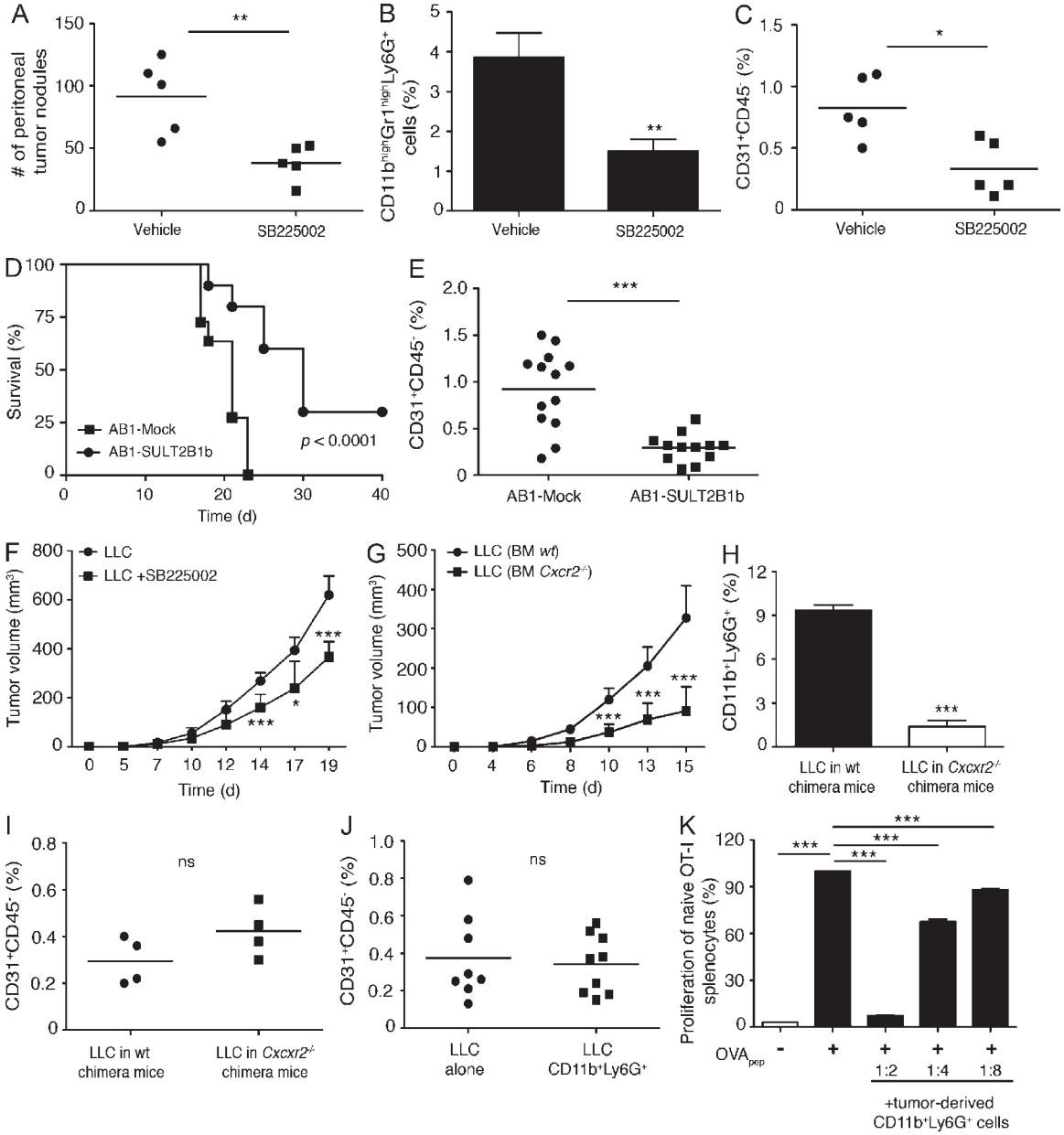

Figure 10. Pharmacologic or genetic CXCR2 inactivation controls tumor growth by reducing angiogenesis and immunosuppression in AB1 and LLC tumor models. (A) Number of peritoneal tumor nodules in AB1-bearing mice treated with vehicle or 0.8 mM SB225002 (n = 5 mice per group). Individual mouse data are shown (mean, horizontal line). **, P = 0.0071. (B) Percentage of CD11b^{high} Gr1^{high}Ly6G$^+$ neutrophils infiltrating AB1 tumors from mice treated with vehicle or with SB225002 (n = 5 mice per group; mean ± SEM). **, P = 0.0045. (C) Percentage of CD45$^-$CD31$^+$ cells in AB1 tumors from mice treated with vehicle or SB225002 (n = 5 mice per group). Individual mouse data are shown (mean, horizontal line). *, P = 0.011. (D) Survival of mice injected with AB1 tumor cells expressing SULT2B1b or mock-transduced. Mean ± SEM of one experiment. Statistical comparison was performed by the log-rank test with 10 mice per group. P < 0.0001. (E) Percentage of CD45$^-$CD31$^+$ cells in AB1-Mock and AB1-SULT2B1b tumors (n = 13). Individual mouse data are shown (mean, horizontal line). Results are representative of two experiments. ***, P < 0.0001. (F) Growth of LLC tumor in mice treated or not with 0.8 mM SB225002 (seven mice per group; mean ± SEM). *, P < 0.05; ***, P < 0.001. (G) Growth of LLC in WT and *Cxcr2*$^{-/-}$ chimera mice. (n = 12–13 mice per group; mean ± SEM). Results are representative of two experiments. ***, P < 0.0001. (H) Percentage of CD11b$^+$Ly6G$^+$ neutrophils infiltrating LLC injected in WT or in *Cxcr2*$^{-/-}$ chimera mice (n = 4 mice per group; mean ± SEM). Results are representative of one out of two experiments. ***, P < 0.0001. (I) Percentage of CD45$^-$CD31$^+$ cells in LLC injected in WT or *Cxcr2*$^{-/-}$ chimera mice (n = 4 mice per group). Individual mouse data are shown (mean, horizontal line). (J) Percentage of CD45$^-$CD31$^+$ cells in LLC tumors alone (n = 8) or coinjected with 22R-HC–migrating neutrophils (n = 9). Individual mouse data are shown (mean, horizontal line). Results are representative of one out of two experiments. *ns*, not significant. (K) Proliferation of OT-I naive splenocytes labeled with the cytosolic dye CFSE and pulsed with the SIINFEKL peptide in the presence of 50% (1:2), 25% (1:4), or 12.5% (1:8) of neutrophils isolated from LLC tumors (mean ± SEM) Results are representative of two experiments. ***, P < 0.0001.

to promote tumor growth. This is confirmed by tumor growth experiments in *Lxrα*$^{-/-}$ bone marrow chimera mice, in which the growth rate of the oxysterol-releasing RMA-Mock is, however, higher than that of RMA-SULT2B1b, where the oxysterols are inactivated (unpublished data). Notably, in our tumor model LXR-β does not seem to play a major role, as RMA-Mock showed the same growth rate in *Lxrβ*$^{-/-}$ and wild-type bone marrow chimera mice (unpublished data). The identification of oxysterols (22R-HC, 20S-HC, etc.) endowed with the promiscuous ability to activate two different receptors highlights the need to carefully investigate these molecules to identify new biological functions associated with oxysterols in different physiological and pathological conditions, including tumors.

The in vivo experiments using 22R-HC–embedded matrigel plugs indicate that oxysterols may contribute, together with CXCL chemokines (Fig. 6 A), to neutrophil recruitment within tumor microenvironment, as indicated by the detection of higher numbers of neutrophils in oxysterol-releasing tumors. These results are further corroborated by the observation that the percentage of neutrophil infiltration correlated with the availability of active oxysterols, but not with the content of CXCL1 and CXCL5 chemokines detected within the tumor (Fig. 6, B and C). Recently, different molecular mechanisms able to modify protein structure within tumors (Nagaraj et al., 2007; Molon et al., 2011) or in damaged tissues (Venereau et al., 2012) have been reported. Particularly, protein nitration has been demonstrated to modify the chemotactic capacity of chemokines present in tumors. In this context, the chemoattractant ability of oxysterols might play a relevant role in the tumor microenvironment, in which chemokines could be structurally and functionally altered (Molon et al., 2011). Whether, this mechanism is also relevant for the recruitment of immune cells in some phases of physiological inflammatory processes (i.e., wound healing) will require further studies.

We report that RMA tumor cells produce 22R-HC and 27-HC oxysterols and other species that we are characterizing (Fig. 1 G), whereas LLC tumor cells produce 24S-HC (not depicted). However, a clear picture of how and when oxysterols are produced within tumor microenvironment remains elusive. RMA and LLC constitutively express transcripts for the oxysterol-generating enzymes *Cyp11a1*, *Cyp27a1*, and *Cyp46a1* (Fig. 1 H and unpublished data; Björkhem, 2002; Mast et al., 2011). However, a nonenzymatic pathway, involving reactive oxygen species that are frequently increased in the tumor microenvironment (Murphy and Johnson, 2008), can also participate in oxysterol generation, further contributing to the production and accumulation of oxysterols in vivo. Moreover, recent studies reveal additional complexity. Indeed, other cells of the microenvironment have been reported to express oxysterol-producing enzymes and to generate oxysterols (Diczfalusy et al., 2009; Yi et al., 2012). Because tumor microenvironment is a complex tissue, in which all the cells described so far to generate oxysterols are present (tumor cells, stromal cells, and immune cells), we speculate that appropriate mouse models are needed to investigate the relative contribution of oxysterol-producing cells within tumors. The investigation of cells and factors regulating oxysterol production should clarify in the near future the mechanisms responsible for oxysterol generation, their overall contribution to tumorigenesis, and possibly identify drugs capable of inhibiting their in vivo generation.

The demonstration that some freshly isolated human tumor cells release oxysterols able to bind both LXR and CXCR2 (Fig. 1 I and J; and not depicted), along with the observation that higher numbers of intratumor neutrophils severely affect overall survival of kidney cancer patients (Jensen et al., 2009), suggests that manipulating LXR ligands and their interaction with CXCR2 and immune cells could provide additional targets for the development of new antitumor therapies.

MATERIALS AND METHODS

Animal studies and reagents. C57BL/6 CD45.1 or CD45.2, Balb/C and NOD-SCID mice were from Charles River and Harlan. *Cxcr2*$^{+/-}$ and *Cxcr2*$^{-/-}$ mice were from The Jackson Laboratory. *Lxrα*$^{-/-}$ knockout mice were generated as described previously (Alberti et al., 2001). Mice were maintained in the pathogen-free facility of San Raffaele Scientific Institute. Experiments were conducted in compliance with the Institutional Animal Care and Use Committee program (IACUC no. 341 and 436). Most antibodies were from BD. CXCL5, CXCL12, CCL3, and IL-8 were from R&D Systems. 22R-HC, 22S-HC, 25-HC, 24,25 Epoxycholesterol, 7β-HC, Cholesterol, chenodeoxycolic acid, and Glyco-CDCA were from Sigma-Aldrich and from Avanti Polar Lipids. 24-HC, 27-HC, 4β-HC, and 7α-HC were from Avanti Polar Lipids. 19-HC was from Santa Cruz Biotechnology, Inc. T0901317 and Pregnenolone were from Cayman. CFSE was used at 4 μM (Molecular Probes). PTX and PTX B-Oligomer were from Enzo Life Sciences. Rat anti–mouse CD11b MicroBeads were from Miltenyi Biotec. SB225002 was from Tocris. Dead Cell Stain kit (Live/Dead Fixable Far red) was from Invitrogen. Buthlyhydroxytoluene (BHT) and solvents of HPLC grade were obtained from Sigma-Aldrich. The C18 cartridges (360 mg) were obtained from Waters Chromatography EUROPE (Netherlands).

Promoter reporter assay for nuclear receptor activity. We transfected 10^5 HEK293 cells/well with 100 ng of the plasmid pMH100X4-TK-luc/well together with 100 ng/well pCMX-Gal4-LXRα plasmid using FuGene 6 Transfection Reagent (Roche). 4 h after transfection, we treated the cells with tumor CM for 24 h. Luciferase activity was evaluated by Luciferase Reporter Assay Systems (Promega) according to the manufacturer's protocol. We used 30 ng β-galactosidase/well for transfection normalization (Villablanca et al., 2010).

Sample collection and solid-phase extraction of hydroxycholesterols. All the cell lines analyzed were seeded at 10^5 cells/ml and cultured for 48 h. Then, conditioned media were collected, added to butylhydroxytoluene (40 μM final concentration) to avoid cholesterol oxidation (Gilardi et al., 2009), and stored at −80°C until processing. Hydroxycholesterol extraction was made as previously described (Burkard et al., 2004). In brief, the C18 cartridges were preconditioned with 1 ml *n*-heptane/2-propanol (50:50, vol/vol), 1 ml methanol, and 2 ml of water. 2 ml of the cell-free medium was then applied to the cartridge using only gravity. Afterward, the cartridge was washed with 4 ml methanol-water (75:25, vol/vol) and briefly dried under vacuum. Hydroxysterols were desorbed with 2 ml *n*-heptane/2-propanol (50:50, vol/vol) using only gravity. The eluted substances were dried at 30°C by evaporation (Rotavapor), and the residue was dissolved in 200 μl of methanol and subjected to CI-MS analysis and HPLC analysis.

MS analysis. MS was performed on a Thermo Electron TRACE DSQTM spectrometer through the rapid heating filament Direct-Exposure Probe (DEP) insertion mode. The MS analyses were performed in chemical ionization (CI-MS) using methane as reactant gas at an electron energy of 70 eV with a source temperature of 200°C.

High performance liquid chromatography (HPLC). An HPLC method was developed based on the HPLC-ESI-MS methods described in McDonald et al. (2007). Hydroxycholesterols were resolved using reverse phase HPLC (RP-HPLC) equipped with a Waters 996 Photodiode Array Detector (wavelength 213 nm). A 100 µl aliquot of lipid extract (in methanol) or standard solution was loaded onto a RP-HPLC column (5 µm, 250 × 4 mm LiChrospher 100 RP18 column; Merck) equipped with a guard column. Elution of hydroxycholesterols was performed at flow rate of 300 µl/min, with a gradient formed by the solvent system A, consisting of methanol/water (85:15, vol/vol) and solvent system B consisting of methanol, both containing 5mM ammonium acetate. The gradient elution program was as follows: for RMA-CM analysis, 3 min with solvent A, 33 min with a linear gradient from 100% solvent A to 100% solvent B, 15 min with 100% solvent B, 5 min with a linear gradient from 100% solvent B to 100% solvent A; for all the other CM analyzed, 3 min with solvent A, 55 min with a linear gradient from 100% solvent A to 100% solvent B, 10 min with 100% solvent B, 5 min with a linear gradient from 100% solvent B to 100% solvent A, and maintained for 10 min to reequilibrate the column before the next run.

Chemotaxis assay. Chemotaxis assays were performed using 5-µm pore polycarbonate filters in a 24-well transwell chamber (Corning Costar Corporation). Total bone marrow or $CD11b^+$ purified cells (2×10^5/100 µl) were seeded in the upper chamber, whereas in the lower chamber 600 µl of medium (RPMI 0.5% BSA) containing 15 µM 22R-HC or 22S-HC or 100 ng CXCL5, CXCL12, CCL3, or IL-8. 2 h later, migrated cells were measured by flow cytometer acquisition of a fixed number of beads (10,000/sample; Polysciences). GPCR involvement was investigated by pretreating the cells for 90 min at 37°C with 500 ng PTX. Desensitization experiments were performed by pretreating the cells for 30-45 min at room temperature with 50 µM 22R-HC or 2 µg/ml CXCL5. 500 ng PTX B-Oligomer was used as control of PTX inhibition. Experiments with SB225002 were performed treating the cells with 20 µM SB225002 before migration. Results of migration experiments were calculated as described previously (Villablanca et al., 2010). Spontaneous migration was always subtracted with the exception of the experiments reported in Fig. 2 (C and D).

Analysis of tumor-infiltrating cells. RMA-Mock, RMA-SULT2B1b, LLC-Mock, and LLC-SULT2B1b tumors have been described previously (Villablanca et al., 2010). AB1-Mock and AB1-SULT2B1b were obtained by engineering AB1 cells with lentivirus encoding SULT2B1b or empty vector as described previously (Villablanca et al., 2010). Tumors collected 14–15 d after injection were cut into small fragments and digested for 45-60 min at 37°C with 1.4 mg/ml collagenase A, B, and D (Roche) and 40 µg/ml DNase (Roche) mixture in RPMI medium with 10% FBS. Single cell suspensions were washed and labeled with Dead Cell Stain kit reagents for 30 min at 4°C. After washing, the cells were incubated for 5 min at RT with Fc-blocking solution (10 µg/ml mouse Fc Block; BD) and labeled with CD11b, Gr1, CD45.1, or CD45.2 mAbs. Samples were run by FACSCalibur flow cytometer (BD) and analyzed by FlowJo software gating on live cells. 10 µM 22R-HC or 22S-HC were administered every 2 d intratumor. After 14 d, collected cells were analyzed as described above.

Real-time RT-PCR experiments. Myeloid cells (immature and mature) were purified by percoll gradients from bone marrow of wild-type mice, or mice injected with RMA-Mock- or RMA-SULT2B1b. Total RNA was isolated with TRIZOL (Invitrogen). Reverse transcription was performed from 1–2 µg of total RNA, using MLV-reverse transcription (Invitrogen). qRT-PCR was performed using real-time PCR (ABI PRISM 7900; Applied Biosystems) and Sybr Green. The comparative Ct method was used to quantify transcripts normalized to *cyclophillin* as a gene reference. qRT-PCR was performed using primers specific for the LXR target genes *Abcg1* and *Srebp-1c*. Primers for *Bv8* have been reported in Shojaei et al. (2007b). Primers for *Cyp11a1*, *Cyp27a1*, and *Ch25h* are as follows: *Cyp11a1* forward, 5′-AGAGTTTCCAAAAGTATGGCCC-3′; reverse, 5′-ATACTGGTGATAGGCCACCCAGG-3′. *Cyp27a1* forward, 5′-GACCTCCAGGTGCTGAAC-3′; reverse 5′-CTCCTGTCTCATCACTTGCTC-3′. *Ch25h* forward, 5′-CTGCCTGCTGCTCTTCGACA-3′; reverse, 5′-CCGACAGCCAGATGTTAATC-3′.

In vivo migration experiments. We injected NOD-SCID mice with RMA-Mock or RMA-SULT2B1b. 13–14 d later, we transferred 10×10^6 CFSE-labeled total bone marrow cells into tumor-bearing mice. 18 h later, tumors were processed as described before. The percentage and number of bone marrow–derived exogenous and endogenous $CD11b^{high}Gr1^{high}$ cells was evaluated by gating on $CFSE^+$ and $CD45.1^+$ cells, respectively.

Parabiosis experiments. 6–8-wk-old sex-matched congenic C57BL/6 wild-type mice were joined at the flanks as described in Wright et al. (2001). 3 d later, 5×10^5 RMA cells were injected s.c. in the flank of the CD45.2 mice. Mice were surgically separated 7, 4, and 2 d prior to collection of tumors and analysis.

Immunofluorescence, immunohistochemistry, and immunocytochemistry. For immunofluorescence, we used anti–CD11b-FITC, biotinylated anti-Gr1 antibody revealed by streptavidin, Alexa Fluor 555 (Invitrogen), and DAPI. We embedded samples in OCT freezing medium and prepared tissue sections 7 mm thick, which were then fixed in 4% paraformaldehyde. Images were taken by the Eclipse i80 microscope (Nikon). For immunohistochemistry, tumor samples were embedded in optimal cutting temperature medium and frozen in liquid nitrogen. We stained 3-µm paraffin sections with H&E for morphological analysis or immunostained them with rat anti-CD31 mAb (Serotec), followed by a biotinylated conjugated rat-specific antibody (Biocare). Reactions were visualized with horseradish peroxidase–conjugated streptavidin and 3,3 diaminobenzidine as chromogen (Biogenex). Slides from LXR ligand migrating $CD11b^{high}Gr1^{high}$ cells were prepared by centrifugation at 1,500 rpm for 10 min in a Shandon Cytospin 3. Cells were stained using May-Grunwald-Giemsa and evaluated under light microscopy.

Matrigel plug assays. 300 µl matrigel containing 0.5 mM 22R-HC or 0.5 mM 22S-HC (100 µl) was injected subcutaneously into C57BL/6 mice. Plugs were removed after 5 h, digested for 1 h at 37°C with 1.8 U/ml Dipsase (Gibco), and analyzed by FACS as described above. 0.8 mM SB225002 was given intraperitoneally 2 d before matrigel injection. Matrigel containing CXCL5, 22R-HC, or 22S-HC alone or together with blocking antibodies against mouse CXCL1, CXCL3, CXCL5, and CXCL7 chemokines (R&D Systems; 10 µg each) was injected subcutaneously into C57BL/6 mice. 5 h later, plugs were removed and analyzed as described above.

CXCL1 and CXCL5 ELISA assays. 7-d-established RMA-Mock and RMA-SULT2B1b tumors were collected and digested mechanically and enzymatically up to single cell suspension. Cells were counted and plated in 24-well plates (10^6 cells/well in 1 ml). After 24 h, supernatants were collected and the content of CXCL1 and CXCL5 was measured according to the manufacturer's recommendations. CXCL1 and CXCL5 ELISA kits were from R&D Systems.

Viral vectors and transduction procedures. The mCXCR2-ΔNGFr lentiviral transfer vector was generated by cloning the murine CXCR2 cDNA in place of the GFP into the self-inactivating hPGK.GFP.wPRE.mhCMV.ΔNGFr.SV40PA lentiviral vector (AgeI–SalI sites). Concentrated VSV-G–pseudotyped LV stocks were produced and titred as described previously (Villablanca et al., 2010). L1.2 cells were transduced with 10^8 or 10^9 transduction units (TU)/ml VSV-G–pseudotyped LV stocks, corresponding to 1.5 or 15 MOI (Villablanca et al., 2010).

Down-regulation of CXCR2. $CD11b^+$ cells were treated with 50 μM of 22R-HC or 22S-HC, 2 μg/ml CXCL5, 1 μg/ml SDF-1α, or 10 μM SB225002 for 30 min at room temperature. After washing, the cells were labeled with anti-CD11b, anti-Gr1, and anti-CXCR2 mAbs and run by FACS.

^{35}S-GTPγS binding assay. Mock- or CXCR2-transduced L1.2 cells were homogenized in 5 mM Tris–HCl and 2 mM EDTA, pH 7.4, and centrifuged at 48,000 *g* for 15 min at 4°C. The resulting pellets (plasma membranes) were washed in 50 mM Tris–HCl and 10 mM $MgCl_2$, pH 7.4, and stored at −80°C until use. The assay was performed as described in de Kruijf et al. (2011) with minor modifications. In brief, aliquots of control or 10 μg CXCR2-expressing membranes were incubated in 96-well plates in assay buffer (20 mM Hepes, 3 mM $MgCl_2$, and 100 mM NaCl, pH 7.4) supplemented with 3 μM GDP, 0.15 nM ^{35}S-GTPγS (1,250 Ci/mmol; Perkin Elmer), and different compound concentrations (10–50 μM). 0.1–50 nM of the CXCR2 agonist IL-8 was also assayed in parallel as a reference compound. SB225002 antagonist was added for 5 min before the addition of IL-8 or 22R-HC to determine the inhibition of the agonist-mediated G protein activation. After incubation at room temperature in a shaking water bath for 60 min, cells were harvested by rapid filtration and assayed for ^{35}S radioactivity. Nonspecific ^{35}S-GTPγS binding was measured with 50 μM GTPγS. Analysis and graphic presentation of ^{35}S-GTPγS binding data were obtained by a nonlinear multipurpose curve fitting computer program (Prism; GraphPad Software).

Measurement of cAMP levels. Intracellular cAMP levels were measured using a competitive binding method (Daniele et al., 2011). In brief, mock- or CXCR2-transduced CHOK1 cells were seeded on 24-well plates (48×10^3 cells/well) in 0.5 ml of medium. After 24 h, the entire medium was removed, and the cells were incubated at 37°C for 15 min with 0.4 ml DMEM in the presence of 20 μM of the phosphodiesterase inhibitor 4-[(3-butoxy-4-methoxyphenyl)-methyl]-2-imidazolidinone (Ro20-1724). The dose–response curve of tested ligands was evaluated by assessing their ability to inhibit cAMP accumulation stimulated by 1 μM forskolin. The compounds were added to cells for 15 min. When required, cells were preincubated for 10 min with SB225002 antagonist. The reaction was terminated by the removal of the medium and the addition of 200 μl of 0.4 N HCl. After 30 min, lysates were neutralized with 50 μl 4 N KOH, and the suspension was centrifuged at 800 *g* for 5 min. For the determination of cAMP production, the cAMP binding protein was incubated with 2 nM [^{3}H]cAMP and 50 μl of cell lysate or cAMP standard (0–16 pmol) at 0°C for 150 min in a total volume of 300 μl. The bound radioactivity was separated by rapid filtration through GF/C glass fiber filters (PerkinElmer Life and Analytical Sciences) and washed twice with 4 ml of 50 mM Tris-HCl, pH 7.4. The radioactivity was measured by liquid scintillation spectrometry.

Receptor binding assay. Competition for the binding of ^{125}I-labeled IL-8 ([^{125}I]IL-8; sp. act., 2,200 Ci/mmol; Perkin Elmer) to mouse L1.2 cells was conducted as described previously (Sozzani et al., 1997). Mock- or CXCR2-transduced L1.2 cells (0.8×10^6/50 μl) in binding medium (RPMI 1640 with 1 mg/ml BSA) were incubated with 0.3 nM of labeled chemokine in the presence of 300 nM of unlabeled IL-8 or 100 μM 22R-HC, 25-HC, 22S-HC, or 4β-HC at 4°C for 2 h. Dose-dependent inhibition experiments were performed by incubating the cells with 100, 50, 10, or 1 μM 22R-HC or 22S-HC. At the end of the incubation, cells were pelleted through a cushion of oil by microcentrifugation. The radioactivity present in the tip of the tubes was evaluated using a gamma counter. Nonspecific binding to L1.2 mock-transduced cells was always subtracted for each condition described.

OT-I proliferation assay. Splenocytes from OT-I mice were labeled with 4 μM CFSE. Then they were washed and pulsed for 1 h at 37°C with 2 μg/ml SIINFEKL peptide. LXR ligand migrating and nonmigrating $CD11b^+$ $Gr1^+$ cells (10^5 or 5×10^4) were cultured in 96-well round-bottomed plates with 2×10^5 CFSE-labeled OT-I splenocytes. 10^5, 5×10^4, and 2.5×10^4 tumor-infiltrating neutrophils were purified using Ly6G-microbeads (Miltenyi Biotec), analyzed by FACS ($CD11b^+Ly6G^+$ were >90% of the cells), and then cultured in 96-well round-bottomed plates with 2×10^5 CFSE-labeled OT-I splenocytes. Cells were analyzed 3 d later with a FACSCalibur flow cytometer with FlowJo software. Data are presented as the percentage of proliferation of SIINFEKL-pulsed, CFSE-labeled OT-I splenocytes relative to the proliferation of SIINFEKL-pulsed, CFSE-labeled OT-I splenocytes alone (set as 100%). To test OT-I memory cells, we harvested OT-I splenocytes from OT-I mice previously immunized (10 d) with 5 μg SIINFEKL peptide emulsified in complete Freund's adjuvant.

Mouse total MMP-9 and Bv8 assays. 22R-HC migrating and nonmigrating cells and fresh splenocytes (2×10^6 cells/ml) were plated in 24-well plates. After 24 h, supernatants were collected and the content of total MMP-9 was measured according to manufacturer's recommendations (mouse total MMP-9; Quantikine; R&D Systems). For Bv8 ELISA assay, we plated 22R-HC migrating and nonmigrating cells in 24-well plates (3×10^6 cells/well in 1 ml) in the absence or in the presence of RMA-CM. After 24 h, supernatants were collected and the content of Bv8 was measured according to manufacturer's recommendations (Bv8 ELISA kit; *Uscn*; Life Science! Inc.).

Angiogenesis assay. We injected mice with 2×10^5 RMA or LLC tumor cells alone or admixed with either 22R-HC migrating $CD11b^{high}Gr1^{high}$ or nonmigrating $CD11b^+Gr1^+$ cells (10^5) resuspended in 100 μl PBS, mixed with 100 μl of matrigel. 6 d later, mice were sacrificed and matrigel plugs collected and digested with 1.4 mg/ml collagenase A, B, and D and 1.8 U/ml Dispase. Cell suspensions were labeled with Dead Cell Stain kit reagents for 30 min at 4°C. After washing, cells were incubated for 5 min at room temperature with Fc-blocking solution (10 μg/ml mouse Fc Block; BD) and labeled with CD31 and CD45 mAbs. We analyzed the samples by FACS (Mazzieri et al., 2011) and considered the endothelial cells as $Dead^-CD45^-CD31^+$ cells. Experiments with B16F1 were performed by injecting 0.5×10^5 B16F1 cells alone or admixed with 5×10^5 BM-purified neutrophils.

Tumor challenge in wild-type, *Cxcr2*$^{-/-}$, *Lxrα*$^{-/-}$, or *Lxrβ*$^{-/-}$ chimera mice. C57BL/6 mice were injected subcutaneously with 1×10^5 RMA, 3×10^5 LLC, or intraperitoneally with 3×10^6 AB1 tumor cells. We evaluated tumor size by measuring perpendicular diameters by a caliper. For AB1 tumors, we evaluated overall survival and the number of peritoneal tumor nodules 14 d after tumor inoculation. Data are reported as the mean tumor volume ± SEM. We gave 0.8 mM SB225002 (Tocris) or DMSO intraperitoneally every 2 d, starting 5 d after tumor infusion. We gave 10 μM 22R-HC intratumor every 2 d. We transplanted lethally irradiated (11 Gy) C57BL/6 mice with bone marrow of *Cxcr2*$^{-/-}$, *Lxrα*$^{-/-}$, *Lxrβ*$^{-/-}$, or WT mice (5×10^6 bone marrow cells/mouse). 6–8 wk later, we challenged mice with RMA with or without SB225002, or with LLC. *Cxcr2*$^{-/-}$ genotype was performed by PCR on splenocytes at the end of the experiments. *Lxrα*$^{-/-}$ or *Lxrβ*$^{-/-}$ genotype was performed by PCR on blood cells before tumor challenge. Because *Cxcr2*$^{-/-}$ chimera mice underwent death during the reconstitution phase, we treated transplanted mice with enrofloxacin for 15 d (7.5 mg/150 μl Baytril 5% solution in 300 ml of drinking water) according to the indication of the veterinary staff of our spf facility.

Neutrophil depletion experiments. C57BL/6 mice were injected subcutaneously with RMA (1×10^5). 7 d later, we performed neutrophil depletion by intratumor injections of 30 μg of purified anti-Ly6G antibody 1A8 (BioLegend) or rat IgG control antibody (Jackson ImmunoResearch Laboratories, Inc.) twice per week, as described in Fridlender et al. (2009). Tumor neutrophil depletion and angiogenesis were evaluated at the end of the tumor challenge by flow cytometry using anti-CD11b, anti-Gr1, anti-CD31, and anti-CD45 mAbs. Tumor growth was analyzed as described above.

Statistical analysis. Data are expressed as mean ± SEM and were analyzed for significance by ANOVA with Dunnet's, Bonferroni's, or Tukey's multiple comparison test, or by Student's *t* test. The analysis was performed with Prism software.

Online supplemental material. Fig. 1 shows the morphological and phenotypic characterization of gated 22R-HC migrating and nonmigrating $CD11b^+Gr1^+$ cells. Online supplemental material is available at http://www.jem.org/cgi/content/full/jem.20130440/DC1.

We are grateful to Alberto Mantovani, Matteo Bellone, and Marco Bregni for helpful and critical discussions. We thank F. Curnis, M. Rocchi, M. Soncini, M. Moresco, and V. Salvi for technical help, and M. Fabbri for providing us with the pRc/CMV plasmid encoding the full-length cDNA of mouse *Cxcr2*.

This work was supported by the Association for International Cancer Research (AICR, UK), Italian Association for Cancer Research (AIRC), and Italian Ministry of Health (RF-2009). E.J. Villablanca was supported by grants from Crohn's & Colitis Foundation of America (CCFA). J.R. Mora was supported by grants from Crohn's & Colitis Foundation of America (CCFA), Cancer Research Institute (CRI), Howard H. Goodman (MGH), Massachusetts Life Science Center (MLSC), and NIH DP2 2009A054301. K.R. Steffensen and J.-A. Gustafsson were supported by grants from the Swedish Science Council (522-2008-3745) and J.-A. Gustafsson from the Robert A. Welch Foundation. A. Paniccia conducted this study as partial fulfillment of the PhD in Biology and Biotherapy of Cancer, Università Vita-Salute San Raffaele (Milan, Italy), and is supported by the Special Program Molecular Clinical Oncology AIRC 5 per mille (9965). C. Traversari and C. Bordignon are employees of MolMed S.p.A.

The authors have no conflicting financial interests.

Submitted: 1 March 2013
Accepted: 21 June 2013

REFERENCES

Acharyya, S., T. Oskarsson, S. Vanharanta, S. Malladi, J. Kim, P.G. Morris, K. Manova-Todorova, M. Leversha, N. Hogg, V.E. Seshan, et al. 2012. A CXCL1 paracrine network links cancer chemoresistance and metastasis. *Cell*. 150:165–178. http://dx.doi.org/10.1016/j.cell.2012.04.042

Alberti, S., G. Schuster, P. Parini, D. Feltkamp, U. Diczfalusy, M. Rudling, B. Angelin, I. Björkhem, S. Pettersson, and J.A. Gustafsson. 2001. Hepatic cholesterol metabolism and resistance to dietary cholesterol in LXRbeta-deficient mice. *J. Clin. Invest.* 107:565–573. http://dx.doi.org/10.1172/JCI9794

Bensinger, S.J., and P. Tontonoz. 2008. Integration of metabolism and inflammation by lipid-activated nuclear receptors. *Nature*. 454:470–477. http://dx.doi.org/10.1038/nature07202

Björkhem, I. 2002. Do oxysterols control cholesterol homeostasis? *J. Clin. Invest.* 110:725–730.

Bronte, V., and P. Zanovello. 2005. Regulation of immune responses by L-arginine metabolism. *Nat. Rev. Immunol.* 5:641–654. http://dx.doi.org/10.1038/nri1668

Burkard, I., K.M. Rentsch, and A. von Eckardstein. 2004. Determination of 24S- and 27-hydroxycholesterol in plasma by high-performance liquid chromatography-mass spectrometry. *J. Lipid Res.* 45:776–781. http://dx.doi.org/10.1194/jlr.D300036-JLR200

Cacalano, G., J. Lee, K. Kikly, A.M. Ryan, S. Pitts-Meek, B. Hultgren, W.I. Wood, and M.W. Moore. 1994. Neutrophil and B cell expansion in mice that lack the murine IL-8 receptor homolog. *Science*. 265:682–684. http://dx.doi.org/10.1126/science.8036519

Corada, M., S. Chimenti, M.R. Cera, M. Vinci, M. Salio, F. Fiordaliso, N. De Angelis, A. Villa, M. Bossi, L.I. Staszewsky, et al. 2005. Junctional adhesion molecule-A-deficient polymorphonuclear cells show reduced diapedesis in peritonitis and heart ischemia-reperfusion injury. *Proc. Natl. Acad. Sci. USA*. 102:10634–10639. http://dx.doi.org/10.1073/pnas.0500147102

Daniele, S., M.L. Trincavelli, P. Gabelloni, D. Lecca, P. Rosa, M.P. Abbracchio, and C. Martini. 2011. Agonist-induced desensitization/resensitization of human G protein-coupled receptor 17: a functional cross-talk between purinergic and cysteinyl-leukotriene ligands. *J. Pharmacol. Exp. Ther.* 338:559–567. http://dx.doi.org/10.1124/jpet.110.178715

de Kruijf, P., H.D. Lim, L. Roumen, V.A. Renjaän, J. Zhao, M.L. Webb, D.S. Auld, J.C. Wijkmans, G.J. Zaman, M.J. Smit, et al. 2011. Identification of a novel allosteric binding site in the CXCR2 chemokine receptor. *Mol. Pharmacol.* 80:1108–1118. http://dx.doi.org/10.1124/mol.111.073825

De Santo, C., R. Arscott, S. Booth, I. Karydis, M. Jones, R. Asher, M. Salio, M. Middleton, and V. Cerundolo. 2010. Invariant NKT cells modulate the suppressive activity of IL-10-secreting neutrophils differentiated with serum amyloid A. *Nat. Immunol.* 11:1039–1046. http://dx.doi.org/10.1038/ni.1942

de Visser, K.E., A. Eichten, and L.M. Coussens. 2006. Paradoxical roles of the immune system during cancer development. *Nat. Rev. Cancer*. 6:24–37. http://dx.doi.org/10.1038/nrc1782

Diczfalusy, U., K.E. Olofsson, A.M. Carlsson, M. Gong, D.T. Golenbock, O. Rooyackers, U. Fläring, and H. Björkbacka. 2009. Marked upregulation of cholesterol 25-hydroxylase expression by lipopolysaccharide. *J. Lipid Res.* 50:2258–2264. http://dx.doi.org/10.1194/jlr.M900107-JLR200

Fridlender, Z.G., J. Sun, S. Kim, V. Kapoor, G. Cheng, L. Ling, G.S. Worthen, and S.M. Albelda. 2009. Polarization of tumor-associated neutrophil phenotype by TGF-beta: "N1" versus "N2" TAN. *Cancer Cell*. 16:183–194. http://dx.doi.org/10.1016/j.ccr.2009.06.017

Fuda, H., N.B. Javitt, K. Mitamura, S. Ikegawa, and C.A. Strott. 2007. Oxysterols are substrates for cholesterol sulfotransferase. *J. Lipid Res.* 48:1343–1352. http://dx.doi.org/10.1194/jlr.M700018-JLR200

Gabrilovich, D.I., and S. Nagaraj. 2009. Myeloid-derived suppressor cells as regulators of the immune system. *Nat. Rev. Immunol.* 9:162–174. http://dx.doi.org/10.1038/nri2506

Gabrilovich, D.I., S. Ostrand-Rosenberg, and V. Bronte. 2012. Coordinated regulation of myeloid cells by tumours. *Nat. Rev. Immunol.* 12:253–268. http://dx.doi.org/10.1038/nri3175

Gilardi, F., B. Viviani, A. Galmozzi, M. Boraso, S. Bartesaghi, A. Torri, D. Caruso, M. Crestani, M. Marinovich, and E. de Fabiani. 2009. Expression of sterol 27-hydroxylase in glial cells and its regulation by liver X receptor signaling. *Neuroscience*. 164:530–540. http://dx.doi.org/10.1016/j.neuroscience.2009.08.003

Grivennikov, S.I., F.R. Greten, and M. Karin. 2010. Immunity, inflammation, and cancer. *Cell*. 140:883–899. http://dx.doi.org/10.1016/j.cell.2010.01.025

Hanahan, D., and R.A. Weinberg. 2011. Hallmarks of cancer: the next generation. *Cell*. 144:646–674. http://dx.doi.org/10.1016/j.cell.2011.02.013

Hannedouche, S., J. Zhang, T. Yi, W. Shen, D. Nguyen, J.P. Pereira, D. Guerini, B.U. Baumgarten, S. Roggo, B. Wen, et al. 2011. Oxysterols direct immune cell migration via EBI2. *Nature*. 475:524–527. http://dx.doi.org/10.1038/nature10280

Herber, D.L., W. Cao, Y. Nefedova, S.V. Novitskiy, S. Nagaraj, V.A. Tyurin, A. Corzo, H.I. Cho, E. Celis, B. Lennox, et al. 2010. Lipid accumulation and dendritic cell dysfunction in cancer. *Nat. Med.* 16:880–886. http://dx.doi.org/10.1038/nm.2172

Janowski, B.A., P.J. Willy, T.R. Devi, J.R. Falck, and D.J. Mangelsdorf. 1996. An oxysterol signalling pathway mediated by the nuclear receptor LXR alpha. *Nature*. 383:728–731. http://dx.doi.org/10.1038/383728a0

Jensen, H.K., F. Donskov, N. Marcussen, M. Nordsmark, F. Lundbeck, and H. von der Maase. 2009. Presence of intratumoral neutrophils is an independent prognostic factor in localized renal cell carcinoma. *J. Clin. Oncol.* 27:4709–4717. http://dx.doi.org/10.1200/JCO.2008.18.9498

Kerbel, R.S. 2008. Tumor angiogenesis. *N. Engl. J. Med.* 358:2039–2049. http://dx.doi.org/10.1056/NEJMra0706596

Liu, C., X.V. Yang, J. Wu, C. Kuei, N.S. Mani, L. Zhang, J. Yu, S.W. Sutton, N. Qin, H. Banie, et al. 2011. Oxysterols direct B-cell migration through EBI2. *Nature*. 475:519–523. http://dx.doi.org/10.1038/nature10226

Mantovani, A., and A. Sica. 2010. Macrophages, innate immunity and cancer: balance, tolerance, and diversity. *Curr. Opin. Immunol.* 22:231–237. http://dx.doi.org/10.1016/j.coi.2010.01.009

Mantovani, A., P. Allavena, A. Sica, and F. Balkwill. 2008. Cancer-related inflammation. *Nature*. 454:436–444. http://dx.doi.org/10.1038/nature07205

Mantovani, A., B. Savino, M. Locati, L. Zammataro, P. Allavena, and R. Bonecchi. 2010. The chemokine system in cancer biology and therapy. *Cytokine Growth Factor Rev.* 21:27–39. http://dx.doi.org/10.1016/j.cytogfr.2009.11.007

Mast, N., A.J. Annalora, D.T. Lodowski, K. Palczewski, C.D. Stout, and I.A. Pikuleva. 2011. Structural basis for three-step sequential catalysis by the cholesterol side chain cleavage enzyme CYP11A1. *J. Biol. Chem.* 286:5607–5613. http://dx.doi.org/10.1074/jbc.M110.188433

Mazzieri, R., F. Pucci, D. Moi, E. Zonari, A. Ranghetti, A. Berti, L.S. Politi, B. Gentner, J.L. Brown, L. Naldini, and M. De Palma. 2011. Targeting the ANG2/TIE2 axis inhibits tumor growth and metastasis by impairing angiogenesis and disabling rebounds of proangiogenic myeloid cells. *Cancer Cell*. 19:512–526. http://dx.doi.org/10.1016/j.ccr.2011.02.005

McDonald, J.G., B.M. Thompson, E.C. McCrum, and D.W. Russell. 2007. Extraction and analysis of sterols in biological matrices by high performance liquid chromatography electrospray ionization mass spectrometry. *Methods Enzymol*. 432:145–170. http://dx.doi.org/10.1016/S0076-6879(07)32006-5

Mellor, A.L., D. Munn, P. Chandler, D. Keskin, T. Johnson, B. Marshall, K. Jhaver, and B. Baban. 2003. Tryptophan catabolism and T cell responses. *Adv. Exp. Med. Biol*. 527:27–35. http://dx.doi.org/10.1007/978-1-4615-0135-0_3

Molon, B., S. Ugel, F. Del Pozzo, C. Soldani, S. Zilio, D. Avella, A. De Palma, P. Mauri, A. Monegal, M. Rescigno, et al. 2011. Chemokine nitration prevents intratumoral infiltration of antigen-specific T cells. *J. Exp. Med*. 208:1949–1962. http://dx.doi.org/10.1084/jem.20101956

Motz, G.T., and G. Coukos. 2011. The parallel lives of angiogenesis and immunosuppression: cancer and other tales. *Nat. Rev. Immunol*. 11:702–711. http://dx.doi.org/10.1038/nri3064

Murdoch, C., M. Muthana, S.B. Coffelt, and C.E. Lewis. 2008. The role of myeloid cells in the promotion of tumour angiogenesis. *Nat. Rev. Cancer*. 8:618–631. http://dx.doi.org/10.1038/nrc2444

Murphy, R.C., and K.M. Johnson. 2008. Cholesterol, reactive oxygen species, and the formation of biologically active mediators. *J. Biol. Chem*. 283:15521–15525. http://dx.doi.org/10.1074/jbc.R700049200

Nachtergaele, S., L.K. Mydock, K. Krishnan, J. Rammohan, P.H. Schlesinger, D.F. Covey, and R. Rohatgi. 2012. Oxysterols are allosteric activators of the oncoprotein Smoothened. *Nat. Chem. Biol*. 8:211–220. http://dx.doi.org/10.1038/nchembio.765

Nagaraj, S., K. Gupta, V. Pisarev, L. Kinarsky, S. Sherman, L. Kang, D.L. Herber, J. Schneck, and D.I. Gabrilovich. 2007. Altered recognition of antigen is a mechanism of CD8+ T cell tolerance in cancer. *Nat. Med*. 13:828–835. http://dx.doi.org/10.1038/nm1609

Nozawa, H., C. Chiu, and D. Hanahan. 2006. Infiltrating neutrophils mediate the initial angiogenic switch in a mouse model of multistage carcinogenesis. *Proc. Natl. Acad. Sci. USA*. 103:12493–12498. http://dx.doi.org/10.1073/pnas.0601807103

Pie, J.E., and C. Seillan. 1992. Oxysterols in cultured bovine aortic smooth muscle cells and in the monocyte-like cell line U937. *Lipids*. 27:270–274. http://dx.doi.org/10.1007/BF02536474

Qian, B.Z., J. Li, H. Zhang, T. Kitamura, J. Zhang, L.R. Campion, E.A. Kaiser, L.A. Snyder, and J.W. Pollard. 2011. CCL2 recruits inflammatory monocytes to facilitate breast-tumour metastasis. *Nature*. 475:222–225. http://dx.doi.org/10.1038/nature10138

Repa, J.J., and D.J. Mangelsdorf. 2000. The role of orphan nuclear receptors in the regulation of cholesterol homeostasis. *Annu. Rev. Cell Dev. Biol*. 16:459–481. http://dx.doi.org/10.1146/annurev.cellbio.16.1.459

Rossi, D., and A. Zlotnik. 2000. The biology of chemokines and their receptors. *Annu. Rev. Immunol*. 18:217–242. http://dx.doi.org/10.1146/annurev.immunol.18.1.217

Shaked, Y., E. Henke, J.M. Roodhart, P. Mancuso, M.H. Langenberg, M. Colleoni, L.G. Daenen, S. Man, P. Xu, U. Emmenegger, et al. 2008. Rapid chemotherapy-induced acute endothelial progenitor cell mobilization: implications for antiangiogenic drugs as chemosensitizing agents. *Cancer Cell*. 14:263–273. http://dx.doi.org/10.1016/j.ccr.2008.08.001

Shojaei, F., X. Wu, A.K. Malik, C. Zhong, M.E. Baldwin, S. Schanz, G. Fuh, H.P. Gerber, and N. Ferrara. 2007a. Tumor refractoriness to anti-VEGF treatment is mediated by CD11b+Gr1+ myeloid cells. *Nat. Biotechnol*. 25:911–920. http://dx.doi.org/10.1038/nbt1323

Shojaei, F., X. Wu, C. Zhong, L. Yu, X.H. Liang, J. Yao, D. Blanchard, C. Bais, F.V. Peale, N. van Bruggen, et al. 2007b. Bv8 regulates myeloid-cell-dependent tumour angiogenesis. *Nature*. 450:825–831. http://dx.doi.org/10.1038/nature06348

Shojaei, F., M. Singh, J.D. Thompson, and N. Ferrara. 2008. Role of Bv8 in neutrophil-dependent angiogenesis in a transgenic model of cancer progression. *Proc. Natl. Acad. Sci. USA*. 105:2640–2645. http://dx.doi.org/10.1073/pnas.0712185105

Sozzani, S., W. Luini, A. Borsatti, N. Polentarutti, D. Zhou, L. Piemonti, G. D'Amico, C.A. Power, T.N. Wells, M. Gobbi, et al. 1997. Receptor expression and responsiveness of human dendritic cells to a defined set of CC and CXC chemokines. *J. Immunol*. 159:1993–2000.

Strieter, R.M., M.D. Burdick, J. Mestas, B. Gomperts, M.P. Keane, and J.A. Belperio. 2006. Cancer CXC chemokine networks and tumour angiogenesis. *Eur. J. Cancer*. 42:768–778. http://dx.doi.org/10.1016/j.ejca.2006.01.006

Vanneman, M., and G. Dranoff. 2012. Combining immunotherapy and targeted therapies in cancer treatment. *Nat. Rev. Cancer*. 12:237–251. http://dx.doi.org/10.1038/nrc3237

Venereau, E., M. Casalgrandi, M. Schiraldi, D.J. Antoine, A. Cattaneo, F. De Marchis, J. Liu, A. Antonelli, A. Preti, L. Raeli, et al. 2012. Mutually exclusive redox forms of HMGB1 promote cell recruitment or proinflammatory cytokine release. *J. Exp. Med*. 209:1519–1528. http://dx.doi.org/10.1084/jem.20120189

Vesely, M.D., M.H. Kershaw, R.D. Schreiber, and M.J. Smyth. 2011. Natural innate and adaptive immunity to cancer. *Annu. Rev. Immunol*. 29:235–271. http://dx.doi.org/10.1146/annurev-immunol-031210-101324

Villablanca, E.J., L. Raccosta, D. Zhou, R. Fontana, D. Maggioni, A. Negro, F. Sanvito, M. Ponzoni, B. Valentinis, M. Bregni, et al. 2010. Tumor-mediated liver X receptor-alpha activation inhibits CC chemokine receptor-7 expression on dendritic cells and dampens antitumor responses. *Nat. Med*. 16:98–105. http://dx.doi.org/10.1038/nm.2074

White, J.R., J.M. Lee, P.R. Young, R.P. Hertzberg, A.J. Jurewicz, M.A. Chaikin, K. Widdowson, J.J. Foley, L.D. Martin, D.E. Griswold, and H.M. Sarau. 1998. Identification of a potent, selective non-peptide CXCR2 antagonist that inhibits interleukin-8-induced neutrophil migration. *J. Biol. Chem*. 273:10095–10098. http://dx.doi.org/10.1074/jbc.273.17.10095

Wright, D.E., A.J. Wagers, A.P. Gulati, F.L. Johnson, and I.L. Weissman. 2001. Physiological migration of hematopoietic stem and progenitor cells. *Science*. 294:1933–1936. http://dx.doi.org/10.1126/science.1064081

Yang, L., L.M. DeBusk, K. Fukuda, B. Fingleton, B. Green-Jarvis, Y. Shyr, L.M. Matrisian, D.P. Carbone, and P.C. Lin. 2004. Expansion of myeloid immune suppressor Gr+CD11b+ cells in tumor-bearing host directly promotes tumor angiogenesis. *Cancer Cell*. 6:409–421. http://dx.doi.org/10.1016/j.ccr.2004.08.031

Yang, L., J. Huang, X. Ren, A.E. Gorska, A. Chytil, M. Aakre, D.P. Carbone, L.M. Matrisian, A. Richmond, P.C. Lin, and H.L. Moses. 2008. Abrogation of TGF beta signaling in mammary carcinomas recruits Gr-1+CD11b+ myeloid cells that promote metastasis. *Cancer Cell*. 13:23–35. http://dx.doi.org/10.1016/j.ccr.2007.12.004

Yi, T., X. Wang, L.M. Kelly, J. An, Y. Xu, A.W. Sailer, J.A. Gustafsson, D.W. Russell, and J.G. Cyster. 2012. Oxysterol gradient generation by lymphoid stromal cells guides activated B cell movement during humoral responses. *Immunity*. 37:535–548. http://dx.doi.org/10.1016/j.immuni.2012.06.015

Zitvogel, L., A. Tesniere, and G. Kroemer. 2006. Cancer despite immunosurveillance: immunoselection and immunosubversion. *Nat. Rev. Immunol*. 6:715–727. http://dx.doi.org/10.1038/nri1936